

Long and short-term flexible control of Power-to-Hydrogen system with terminal cost function and flexibility envelope

Josien H.L. de Koning

Master's Thesis

Automatic Control Laboratory
Swiss Federal Institute of Technology (ETH) Zurich

Supervision

Prof. John Lygeros (ETH)
Dr. Hanmin Cai (EMPA)
Dr. Binod Koirala (EMPA)

May 2023

<i>Project type:</i>	MA
<i>Project title:</i>	Energy flexible community with electrolyser and fuel cell
<i>Student:</i>	Josien H.L. de Koning (jdekoning@student.ethz.ch)
<i>Supervisor:</i>	Dr. Hanmin Cai (hanmin.cai@empa.ch) Dr. Binod Koirala (binod.koirala@empa.ch)
<i>Supervising professor:</i>	Professor John Lygeros
<i>Semester:</i>	Autumn 2022
<i>Start date - end date:</i>	03.10.2022 - 17.04.2023
<i>Office space:</i>	Not required, office space provided at EMPA

Project description

Integration of distributed renewable energy resources (RES) and ongoing electrification of heating and mobility sectors put strains on the operation of power systems, which was planned without accounting for such operation. A large amount of research has focused on short-term flexibility in a matter of hours by exploiting thermal inertia of building envelopes[1]. Meanwhile, energy-autarkic buildings¹² implementing electrolyser and fuel cell setups start to emerge and provide additional flexible components for operational flexibility at the distribution system level. Additionally, such setup can potentially provide both short-term and long-term flexibility as well as enhance the resilience of the community. However, this advantage comes at the cost of efficiency. Finally, the models [2] of the systems need to balance between accuracy and computational complexity when accounting for real-time optimal control and approximation of long-term flexibility needs.

Currently, a systematic evaluation of flexibility potential of such setup and the utility function [3] is missing. However, such evaluation is critical for strategic flexibility planning and business model development. Therefore, the aim of this project is to develop control-oriented models that exploit both short- and long-term flexibility. The trade-off between conversion efficiency and flexibility offering is a core analysis.

Tasks

1. Literature review on electrolyser models, flexibility services and flexibility indicators.
2. Analysis of historical electrolyser data³ collected at move⁴ of EMPA and model the controlled system.
3. Develop control-oriented model of electrolyser based on historical data and existing models.
4. Develop model predictive control (MPC) for a grid-connected building with photovoltaics and power-to-hydrogen-to-power (P2H2P) system.

¹<https://www.umweltarena.ch/ueber-uns/architektur-und-bauprojekte>

²<https://www.homepowersolutions.de/en/product/>

³<https://info.nestcollaboration.ch/wikipediapublic/data/>

⁴<https://move.empa.ch/>

-
5. Assess flexibility potentials with the selected flexibility indicators while considering uncertainties.
 6. Write thesis.
-

Timeline

- Month 1: (1) Analysis of historical electrolyser data collected at move of EMPA and model the controlled system.
 - Month 2: (2) Develop control-oriented model of electrolyser based on historical data and existing models.
 - Month 3: (3) Develop model predictive control (MPC) for a grid-connected building with photo-voltaics and power-to-hydrogen-to-power (P2H2P) system.
 - Month 4: (4) Develop model predictive control (MPC) for a grid-connected building with photo-voltaics and power-to-hydrogen-to-power (P2H2P) system.
 - Month 5: (5) Assess flexibility potentials with the selected flexibility indicators while considering uncertainties.
 - Month 6: (6) Write thesis; final report and presentation
-

Procedures

1. The student and supervisor will follow the checklists "*Procedures for Students*" and "*Procedure for Supervisors*", available from the *Internal* section of the Automatic Control Lab website.
 2. The student and supervisor will hold weekly meetings at an agreed time. This does not exclude the possibility of additional discussion outside these meetings, should these be required.
 3. The student should keep adequate notes throughout the project to assist in preparation of the final report. It may be useful to maintain draft material in \LaTeX form for direct use in the report.
 4. At the end of the project, the student must submit a final report of length no more than 50 pages, and hold a seminar of length 20 minutes at the Automatic Control Lab.
 5. Code has to be properly commented and handed over at an agreed time together with the final report by a GitLab repository (EMPA requirement).
-

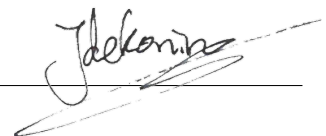
Signatures

Student

Name Josien de Koning

Date 06.09.2022

Signature



Abstract

Hydrogen has been identified as an important energy carrier in future low-carbon energy systems. It has potential for long-term energy storage as well as decarbonization of hard-to-abate sectors. Moreover, it can provide flexibility to the electricity grid through electrolyzers and fuel cells. The future electricity system is in need of more flexibility due to the increase of intermittent energy sources and the seasonal imbalance between energy supply and demand. This thesis proposes a Model Predictive Control (MPC) algorithm for the flexible operation of a Power-to-Hydrogen system under day-ahead electricity market prices. A piece-wise linear value function is generated from offline optimization using the Stochastic Dual Dynamic Programming (SDDP) algorithm. It is then added to the MPC objective to take into account the long-term horizon. In order to represent the flexible operation more accurately, the cold start-up of the electrolyser is included in the model. Finally, the short-term flexibility of the system is assessed using a flexibility envelope using the optimal trajectory resulting from the MPC. As such, the whole chain from long-term to short-term flexibility is addressed. The developed methodology is then applied to the MOVE demonstrator (hydrogen refuelling station with on-site hydrogen production from an electrolyser and photovoltaics) at EMPA in Dübendorf, Switzerland.

Acknowledgements

I would like to list the people that have helped me complete this Master Thesis. Binod Koirala and Hanmin Cai helped me with their excellent supervision. Timo Laaksonlaita did a Master Thesis about MOVE a few years before me and his report was of great help, allowing me to spend time on extending on his conclusions. Adrian Gonzales and Sascha Stoller provided background information on the MOVE system and helped me with the technicalities of the ehub platform. I would like to thank Marta Fochesato, Julie Rousseau and Gabrielle Humbert for being guest during my midterm presentation and providing valuable feedback. Marta was also of great help with an introductory meeting in the beginning, while Julie helped me to understand electricity markets. All other colleagues at the EMPA Urban Energy Systems Group made sure I enjoyed my lunches. Sabrina Baumann was of great help in the administrative process of the thesis. Of course, many thanks go to Prof. John Lygeros for providing grading and final assessment.

Contents

Abstract	4
Acknowledgements	5
List of Figures	8
List of Tables	11
List of Acronyms	12
List of Terms	13
1 Introduction	14
1.1 Energy flexibility	14
1.1.1 Variability characteristics	14
1.1.2 Flexibility needs	16
1.1.3 Flexibility providers	16
1.1.4 Flexibility market	17
1.1.5 Flexibility metrics	17
1.1.6 Flexibility challenges	18
1.2 Hydrogen	18
1.2.1 Flexibility of electrolyzers	19
1.2.2 Literature review on flexible control of Power-to-Hydrogen(-to-Power) systems . .	19
1.3 Control of flexible energy systems	20
1.4 Thesis outlook	21
1.4.1 Research gap and objectives	21
1.4.2 Research Methods and Thesis structure	21
2 Model	23
2.1 Hydrogen pressure, temperature and density	24
2.2 Electrolyser	24
2.2.1 Transient behaviour	25
2.2.2 Control of mass flow	26
2.2.3 Relationship between mass flow and power	27
2.3 Hydrogen storage tanks	29
2.4 Compressors	30
2.5 Hydrogen demand	31
2.5.1 Amount of refuelling events	32
2.5.2 Time of refuelling events	33
2.5.3 Amount refuelled	33
2.5.4 Statistical model	33
2.6 PV production and predictions	35
2.7 Day-ahead electricity prices	35
3 Control Algorithm	36
3.1 Terminal cost function	36
3.2 Dual Dynamic Programming	37

3.2.1	Application to MOVE	39
3.2.2	Results	40
3.3	Stochastic Dual Dynamic Programming	42
3.3.1	Results	43
3.4	Model Predictive Control	46
3.4.1	Correction of control signals	48
3.4.2	Deterministic MPC with perfect foresight	49
3.4.3	Deterministic MPC with imperfect foresight	50
4	Flexibility Assessment	51
4.1	Flexibility Envelope	51
4.1.1	Maximizing power	51
4.1.2	Minimizing power	52
4.1.3	Combined flexibility envelope	53
5	Conclusion and Discussion	55
5.1	Conclusion	55
5.2	Limitations and future work	55
	Bibliography	59

List of Figures

1.1	Basic concepts of variability. (a) and (b): Variability occurs at different timescales and has both deterministic and stochastic elements. It occurs in supply as well as demand. (c): For stagewise-dependent variability, the power prediction error decreases over time but a small uncertainty band always remains	15
1.2	Flexibility needs related to relevant timescales and spatial scales. [18]	16
2.1	Schematic overview of MOVE. For simplicity, several components are not shown: the battery trailer, EV charging station and CNG fueling station, since they are not relevant for this thesis; the HCNG fueling station, since it is only used for one experimental vehicle. A fuel cell is not present in move, but modelled as a virtual technology.	23
2.2	Comparison of ideal gas law and Lemmon equation. The right figure shows the pressure range of all tanks while the left graph is a zoom-in on the pressure range of the 30 bar tank. The line color represents different temperatures. Opaque lines represent the Lemmon equation while more transparent lines represent the ideal gas law.	24
2.3	Simplified representation of the electrolyser in MOVE. It shows the subsystems, the control system and the most relevant sensors. Most subsystems also have a cooling system and a power supply, which are not shown for the sake of readability. Oxygen is emitted into the environment.	25
2.4	Electrolyser behaviour in time and model equivalents. Although the shutdown is normally immediate, this specific case shows a shutdown due to high pressure in the 30 bar buffer.	26
2.5	Relationships for the control of electrolyser mass flow. The underlying data is shown in black while the fitted curves are shown in blue.	27
2.6	Relationship between mass flow and power of the electrolyser. The underlying data is shown in black while the fitted curves for the MILP optimization model are shown in color. The relationship in the right graph is the combination of the two relationships in the graphs on the left.	28
2.7	HHV efficiency of MOVE electrolyser. The underlying data is shown in black while the orange line shows the efficiency according to the piecewise-linear mass flow to power relationship (Eq.2.7). The meaning of auxiliary, voltage and Faraday efficiency are explained by Eq. 2.8-2.10	28
2.8	Buffer temperature	29
2.9	Power and mass flow of compressors.	30
2.10	Details of the 440 bar compressor. Left: Two distinct compressor speeds based on the pressure in the 30 bar tanks. Right: Efficiency is strongly dependent on target pressure.	31
2.11	Average number of 700 bar refuelling events per day (centered rolling window of 8 weeks)	32
2.12	Relationship between the average number of cars per day during an entire week and the average number of cars during work/free days in the same week.	32
2.13	Probability distributions for the amount of cars refueling per day. Several periods with relatively stationary behaviour (refer to Fig. 2.11) are analysed separately. The blue bars show the empirical distribution, while the red lines show the results from the Poisson distribution. Based on visual inspection of the figure, the Poisson distribution is sufficiently accurate.	33
2.14	Empirical probability distribution P_T for the arrival time of cars. The bin size is 1 hour. A uniform distribution is assumed within each bin.	33
2.15	Empirical probability distribution P_M for amount of hydrogen refueled by a car. The bin size is 0.25 kg. A uniform distribution is assumed within each bin.	34

2.16	Photovoltaic panels included in the MOVE-system. There is 549 m ² of roof PV and 84 m ² of façade PV, resulting in a total capacity of 73 kWp.	35
2.17	Day-ahead prices from the ENTSO-E Transparency Platform [14]. Prices after April 2021 are not used since those prices are atypical.	35
3.1	Flowchart of the proposed flexible control algorithm. The SDDP algorithm addresses timescales longer than a week. It performs an offline optimization of the single-stage, linear model over a time horizon of 485 days with hourly resolution and produces a set of terminal cost functions. Timescales shorter than a week are addressed by online MPC. The Optimal Control Problem (OCP) is a MILP optimization problem that optimizes the three-stage mixed-integer linear model of MOVE over a horizon of 7 days with hourly resolution. After optimization, the control signals are corrected and applied to the plant, which is the non-linear simulation model in this thesis. Measurements from the simulation are used as the initial states of the OCP in the next timestep.	36
3.2	Flowchart of the Dual Dynamic Programming (DDP) algorithm, slightly simplified for the sake of understandability. First, all approximate terminal cost functions $\hat{V}_t(x_t)$ are initialized as zero. Then, the forward simulation iterates forward through the timesteps and finds the optimal trial values \hat{u}_t and \hat{x}_{t+1} . Then, the backwards recursion iterates through the timesteps in reverse. Each subproblem is solved and the dual solution is used to add a hyperplane to the terminal cost function. This terminal cost function is then used in the previous subproblem, etc. The algorithm is stopped when the total cost of the forward simulation (upper bound) and the terminal cost function of the first timestep (lower bound) are sufficiently close together.	38
3.3	Piecewise-linear, convex terminal cost function.	39
3.4	DDP results: simulation of optimal policy over 16 months.	41
3.5	DDP results: simulation of optimal policy over 16 months, zoomed in on a week in May/June. There are 6 full discharges of the storage in 2019.	41
3.6	DDP results: marginal value of stored hydrogen. The marginal value indicates the decrease in terminal cost when the fill level is increased by 1 kg, departing from the fill level indicated by the color. The drop in marginal value around Jan 2020 is due to lower energy prices during the winter holidays. The marginal values after 1 Jan 2020 should not be used since they are too close to the end of the horizon.	42
3.7	Markovian policy graph of the SDDP model of MOVE. Each square represents one timestep t and one Markov state s . The columns represent timesteps. The rows represent the different Markov states, in this case the different years of historical data. Each row of historical data consists of day-ahead electricity prices C_{da} and PV power P_{pv} . The wiggly lines represent the discrete probability distribution for hydrogen demand that is applied separately to each timestep since it is stagewise-independent. The straight and curved arrows represent the probability of transitioning between nodes. The transition probability is chosen such that on average, there is a switch between Markov states every 10 days. The circle represents the root node. There is an equal probability of switching from the root node to each row of historical data, so that all historical years are equally represented. A random initial mass is applied to the root node so that all storage fill levels are explored in the beginning of the year.	43
3.8	SDDP results: simulation of optimal policy over 16 months. Black lines show the simulated path while the grey lines show the realizations of the other historical years that have been used to find the optimal policy. The bottom plot shows the storage level of the aggregated hydrogen tank. The top plot shows the markov state, i.e. the year that is sampled at a certain timestep.	44
3.9	SDDP results: marginal value of stored hydrogen. The marginal value indicates the decrease in terminal cost when the fill level is increased by 1 kg, departing from the fill level indicated by the color. The drop in marginal value around Jan 2020 is due to lower energy prices during the winter holidays. Around July and October, the low storage levels show no spikes in marginal value. This is because low storage states were explored in none of the scenarios during this period.	44
3.10	Correction of the activation signal before it is applied to the plant.	48
3.11	Optimization results for a week in May/June	49
3.12	Overview of inputs to the Optimal Control Problem in case of imperfect foresight.	50

4.1	Flexibility envelope for a week in May-June. The colors represent the maximum duration for which a power level can be guaranteed, when initialized with the state variables in the corresponding timestep. The white areas indicate power levels are either (a) infeasible or (b) might be feasible, but cannot be guaranteed. The standard power level is the planned power level that will happen when no flexibility requests occur.	53
-----	---	----

List of Tables

1.1	Overview of flexibility types, timescales and methods addressed in this thesis and their corresponding sections in the thesis.	22
2.1	Properties of the storage tanks	29
2.2	Compressor information	31
2.3	Discrete probability distribution for amount of hydrogen tanked on a workday from 12:00-13:00.	34

List of Acronyms

AC Alternating Current
aFFR Automatic Frequency Restoration Reserve
BoP Balance of Plant
CNG Compressed Natural Gas
DC Direct Current
DDP Dual Dynamic Programming
DSO Distribution System Operator
EMPA Eidgenössische Materialprüfungs- und Forschungsanstalt
EV Electric Vehicle
FCEV Fuel Cell Electric Vehicle
HCNG Hydrogen Compressed Natural Gas
HHV Higher Heating Value
LHV Lower Heating Value
LP Linear Program
mFFR Manual Frequency Restoration Reserve
MILP Mixed-Integer Linear Program
MPC Model Predictive Control
OCP Optimal Control Problem
P2H Power-to-Hydrogen
P2H(2P) Power-to-Hydrogen(-to-Power)
P2H2P Power-to-Hydrogen-to-Power
PCR Frequency Containment Reserve
PEM Proton Exchange Membrane or Polymer Electrolyte Membrane
PV photovoltaics
SDDP Stochastic Dual Dynamic Programming
TSO Transmission System Operator

List of Terms

electrolyser Electrochemical device that performs electrolysis, i.e. converts electricity and water into hydrogen and oxygen. Alternative spelling: electrolyzer

fuel cell Electrochemical device that performs converts hydrogen and oxygen into water and electricity with a typical efficiency of ... %. It is the reverse process of electrolysis.

MOVE A future mobility demonstrator at the research institute Eidgenössische Materialprüfungs- und Forschungsanstalt (EMPA) in Dübendorf, Switzerland, has such a hydrogen system

Chapter 1

Introduction

The utilization of fossil fuels within energy systems has given rise to a host of issues. Firstly, fossil fuels cause greenhouse gas emissions, resulting in global warming. Secondly, they are a finite resource. Thirdly, their uneven geographical distribution results in certain regions being overly reliant on others for their energy needs. Consequently, the international community largely agrees on a transition towards a low-carbon energy system, in which energy demand is reduced and fossil fuels are replaced by renewable energy sources [8].

Electricity can be a suitable low-carbon energy carrier if it is produced by major renewable energy generators such as wind turbines, hydro turbines and solar photovoltaics (PV). Its drawback is that, unlike gas pipelines, electric cables have no storage capacity—they transmit electricity instantaneously. Therefore, *electricity supply and demand in the electric grid have to match at all time scales*. As various sectors such as heating and transport are being electrified to reach decarbonisation targets, the amount of electricity transmitted through the grid is growing. At the same time, the increasing share of wind and solar energy is intermittent and non-dispatchable, unlike the traditional power sources that they replace. Therefore, it is becoming increasingly challenging to match supply and demand in the electric grid. Energy flexibility—the ability of an energy system to manage variability in energy supply and demand—is increasingly needed to achieve this balance.

Hydrogen has also been identified as an important energy carrier in future low-carbon energy systems. In particular, it has potential for seasonal energy storage and for the decarbonization of hard-to-abate sectors such as the aviation, chemical and steel industry [29]. Green hydrogen is produced in an electrolyser, which turns electricity and water into hydrogen and oxygen. This sector-coupling between hydrogen and electricity can provide much needed flexibility to the electric grid [21].

The goal of this thesis is to perform a flexibility assessment and develop a control scheme that exploits the flexibility of Power-to-Hydrogen(-to-Power) systems with PV and electrolyser in the context of an energy community with hydrogen demand and building energy demand. The thesis is a case study on MOVE, the future mobility demonstrator at Eidgenössische Materialprüfungs- und Forschungsanstalt (EMPA). In the rest of the introduction section, the literature review is presented. In Chapter 2 Model, a model of a Power-to-Hydrogen system is established. Then, in Chapter 3 Control, a flexible control algorithm is proposed. In Chapter 4 Flexibility Assessment, the flexibility of the Power-to-Hydrogen system is assessed. The thesis ends with a conclusion and outlook.

1.1 Energy flexibility

Energy flexibility is an umbrella term that is lacking a unified definition. In general, *energy flexibility describes the ability of an energy system or component to manage (expected or unexpected) variability in energy supply and demand at different time scales*[18]. This section discusses several aspects of flexibility.

1.1.1 Variability characteristics

Variability refers to fluctuations in electricity supply and demand, which can create imbalances. To better understand flexibility, it is needed to understand several important characteristics of variability first.

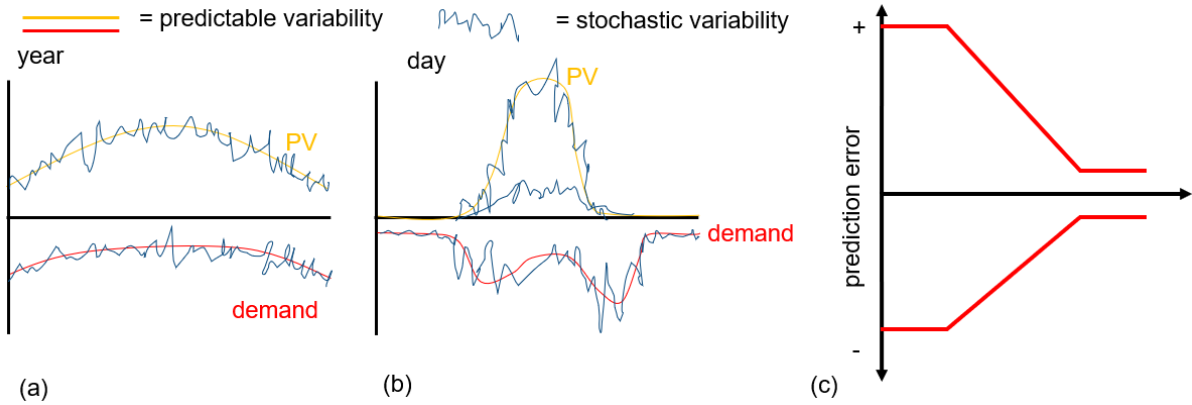


Figure 1.1: Basic concepts of variability. (a) and (b): Variability occurs at different timescales and has both deterministic and stochastic elements. It occurs in supply as well as demand. (c): For stagewise-dependent variability, the power prediction error decreases over time but a small uncertainty band always remains

Supply vs demand Variability occurs both at the supply and the demand side, for example fluctuations in solar energy and fluctuations in space heating demand for buildings.

Predictability Variability can be categorised into *deterministic variability* and *stochastic variability*. Deterministic variability refers to expected patterns that are known years beforehand. Examples include the increase in heating demand in winter, the seasonal and day-night cycles of solar energy and the relatively lower electricity demand during weekends. The knowledge of these expected patterns stays constant as time nears. On the other hand, stochastic variability is seemingly random and not fully known beforehand, such as the occurrence of windy and windless days or a power plant breaking down. It can be subdivided into *stagewise-dependent variability* and *stagewise-independent variability*.

Stagewise-dependent variability depends on past events and can therefore be predicted based on measurements. As time nears, these predictions become more accurate, although they may never be fully accurate. The weather is an excellent example of stagewise-dependent variability, as weather forecasts predict the weather based on the current and past states of the atmosphere. In contradiction, stagewise-independent variability does not depend on past events. An example is hydrogen demand for vehicle refuelling, as the arrival of one car does not affect the chance of arrival of a next car. While it is possible to make some prediction based on the average arrival pattern, the prediction cannot be improved as time draws near.

Time scale Variability occurs at different time scales, from seconds to years. At the (sub-)second scale, a generator or interconnector may abruptly break down. At the minute to hour scale, there are deviations between the actual and forecasted electricity demand and supply. For example, the wind may pick up or people start cooking earlier than expected. At the daily scale, there are expected fluctuations such as the peak of electricity demand in the evening and the daily fluctuation in solar irradiation. At the (multi-)week scale, there are week-weekend patterns in energy demand and spells of weather. These weather spells can last anywhere from a day to a few weeks and can only be predicted from a limited time in advance. At the yearly scale, variability is caused by the annual cycle of seasons. In particular, there is much more solar energy available in the summer than in the winter, while heating demand shows a reverse pattern. Hydropower and wind energy also show seasonal patterns. Variability can even be observed at the multi-year scale. This includes trends such as climate change and increasing e-charging demand for electric vehicles.

Spatial scale Variability occurs at different spatial scales. A single cloud shading a photovoltaic roof is very local and compensated by nearby roofs that may not be shaded at that moment. On the other hand, the summer-winter cycle causes a comparable variability pattern in entire Europe. While the first may cause local problems, the latter affects the entire European energy system.

Coupling Most variability in energy systems is (partially) coupled. For example, both space cooling demand and PV production are increased during sunny afternoon hours, compensating for each other. In the winter, heating demand is increased while PV production is decreased. In this case, the coupling worsens the energy imbalance. On the other hand, hydrogen vehicle refuelling demand is not strongly coupled to the weather.

1.1.2 Flexibility needs

Flexibility is needed to successfully operate the electricity grid. Switzerland is part of the synchronous grid of Continental Europe, a fully interconnected, 50 Hz Alternating Current (AC) electricity network. Countries and regions are interconnected by the transmission grid, a set of high voltage lines that transport electricity over larger distances. The transmission grid is managed by one or a few Transmission System Operators (TSOs) in each country. In Switzerland, the TSO is Swissgrid. Distribution grids are local, lower-voltage electricity networks that connect consumers and smaller generators. Distribution grids are connected to the transmission grid and managed by Distribution System Operators (DSOs). Balancing supply and demand in this grid is not only needed to satisfy electricity demand, but also to ensure safe operation. Four different flexibility needs can be identified[18] (Fig. 1.2):

Flexibility for Energy refers to the basic requirement of satisfying electricity demand and ideally, preventing curtailment of supply. It is applicable to imbalances that can be predicted some time beforehand. The relevant activation timescale is hours to years.

Flexibility for Power refers to the short term need of balancing electricity supply and demand. If supply and demand are out of balance, the grid frequency, which is synchronous throughout Continental Europe, starts deviating from 50 Hz. If the deviation is too large, protection will disconnect equipment to prevent damage, eventually leading to a blackout. Flexibility for Power differs from Flexibility for Energy in that it has to activate at much shorter timescales, namely sub-second to hour. It applies to stochastic variability and is caused by short-term prediction errors in supply and demand.

Flexibility for Transfer Capacity refers to flexibility needed to prevent overloading of electricity lines and equipment. It is of a spatial nature, as the overloading of a line can be mitigated by transmitting electricity via a different route through the electricity network.

Flexibility for Voltage refers to flexibility to control voltage and reactive power. Reactive power occurs when AC voltage and current are out of phase with each other, an effect caused by certain network elements, electric generators and consumers. There is a direct relationship between reactive power and voltage. Generation and consumption of electricity can lead to local voltage drops and rises in the distribution grid. Reactive power needs to be injected into the grid at specific locations to correct the voltage level[4]. The decentralization of power generation and increase of local electricity demand peaks leads to different voltage patterns and increased need for voltage support.

This thesis focuses on *Flexibility for Energy* and *Flexibility for Power*.

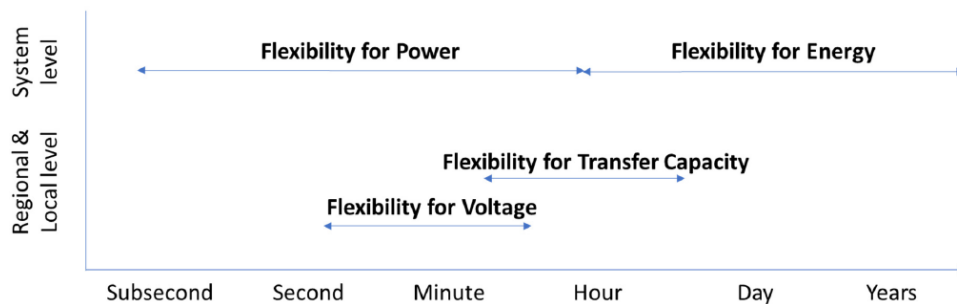


Figure 1.2: Flexibility needs related to relevant timescales and spatial scales. [18]

1.1.3 Flexibility providers

Flexibility is provided by adjusting electric supply or demand in the direction that helps restore the balance in the electric system. Several methods for providing flexibility can be distinguished.

Supply Lowering or increasing energy supply by dispatchable generators such as gas and hydropower turbines, or renewable energy curtailment.

Demand Preponing or postponing electric loads (load shifting), or canceling loads altogether (load shedding).

Storage Overcoming temporal mismatches in supply and demand by charging and discharging and an energy storage.

Sector-coupling Converting electricity into another energy carrier, such as heat or hydrogen. This conversion can be flexibility adjusted to run at times when electricity is available and cease when electricity supply gets low. The existence of a heat or hydrogen demand is a precondition.

Grid interconnection Exchange of electricity with neighbouring electric grids.

1.1.4 Flexibility market

Flexibility for Energy is currently enabled through electricity markets. In Europe, the electricity system has been largely liberalized, allowing energy companies to buy or sell electricity on the electricity market. Electricity can be traded far in advance, but the main market is the day-ahead electricity market, where electricity is traded for each hour of the following day. After that, adjustments can be made by trading electricity on the continuous intra-day market, which closes minimum 5 minutes before the moment of delivery. The electricity market ensures that supply and demand are matched ahead of time.

Flexibility for Power is enabled through the balancing market. The TSO buys control power reserves on the balancing market. These are power bands that the reserve seller can turn on or off at a signal of the TSO. The TSO continually uses these reserves to balance short-term stochastic mismatches between supply and demand, consequentially bringing the grid frequency back to 50 Hz. The balancing market is split up into 3 products: Frequency Containment Reserve (PCR), which has to be fully available in 30 seconds and lasts for max. 15 minutes; Automatic Frequency Restoration Reserve (aFFR), which has to be fully available in 5 minutes and typically lasts max. 15 minutes; and Manual Frequency Restoration Reserve (mFFR), which has to be fully available in 15 minutes and can last up to 4 hours [19]. Very short-term stochastic mismatches in supply and demand are currently absorbed by the rotational inertia of large, traditional generators. As traditional generators disappear, alternatives (*virtual inertia*) need to be developed to provide this short term flexibility.

Traditionally, only large stakeholders can participate in the electricity and balancing market. However, it is desirable to use the flexible assets of smaller prosumers as well. Aggregators, enabled by digitalization, pool these assets together into a virtual power plant that participates in the electricity or balancing market. Therefore, the rest of this thesis assumes no size restrictions for participation in the electricity and balancing market.

1.1.5 Flexibility metrics

Since there is so many subcategories of variability and flexibility, there does not exist one single flexibility indicator. Instead, a multitude of indicators has been used. Yet, it is important to have common metrics to enable remuneration and flexibility assessment. For designing flexible energy systems, it is firstly important to look at non-aggregated indicators such as minimum and maximum power levels, energy storage size, reaction time, cost, cost of ramping loads, cost of start-up, cost of shut-down, standby cost, exergy loss, etc.

In the context of buildings with in-house energy production, self-sufficiency and self-consumption have been widely used to indicate flexibility [27]:

$$self - sufficiency = 1 - \frac{energy\ imports}{energy\ consumption} \quad (1.1)$$

$$self - consumption = 1 - \frac{energy\ exports}{energy\ production} \quad (1.2)$$

Interested readers are referred to [27] for a more extensive review of flexibility metrics and remuneration schemes for demand response programs. For PCR, aFFR and mFFR, the flexibility metric is the power level that can be sustained for a certain duration within a certain reaction time to full power.

Under the assumption of a perfect market, the day-ahead electricity prices can be interpreted as the cost or value of electricity at any hour. This means that the day-ahead price signals can be used as an indicator for flexibility. Since day-ahead prices are decided 12 - 36 hours before the delivery moment, they are only a metric for *Flexibility for Energy*, i.e. day-ahead cost indicates flexibility for deterministic variability and stagewise-dependent stochastic variability for which a relatively good forecast can be generated 36 hours beforehand. Day-ahead cost is used in this thesis to assess *Flexibility for Energy*.

For short-term flexibility, Gasser et al. [16] propose the *flexibility envelope* concept. The flexibility envelope is applied to a building in [7]. The flexibility envelope communicates the duration that certain power levels can be sustained, assuming the initial conditions of a certain timestep. The flexibility can comprehensively communicate the available flexibility with a DSO or virtual power plant, who can then give a signal to the power system to assume a certain power level. Remuneration schemes are not yet discussed in flexibility envelope research. In this thesis, the flexibility envelope will be used to assess *Flexibility for Power* in Chapter 4.

1.1.6 Flexibility challenges

One might wonder why the flexibility challenge cannot simply be solved by storing electricity. This is because energy storage is generally expensive. It is cheaper to produce electricity when it is needed, and consume electricity when it is available, since the costs of additional storage devices are avoided. In its pure form, electrical energy only be stored in a financially viable way for a very short amount of time, for example in (super-)capacitors. Otherwise, electricity needs to be converted into another form of energy to be stored more cheaply, for example in batteries, hydro reservoirs or as hydrogen. But these methods are still more expensive than consuming the electricity directly [29].

For day-night energy storage, the energy amount are quite low and the storage is used for 365 cycles per year. On the other hand, seasonal energy storage requires a very large amount of energy to be stored and has only one cycle per year. These high energy capacity needs make seasonal storage very challenging. Not only should the cost per stored unit of energy (p.e. kWh) be low, but also the space use and availability of materials is important. Due to these reasons, batteries fail as a suitable candidate for seasonal storage. Hydro-reservoirs are used as seasonal storage but take a lot of space. Generally, not enough space is available to cover the entire seasonal imbalance. Furthermore, the potential for expanding hydro-reservoirs is limited.

1.2 Hydrogen

Green Hydrogen is currently gaining traction as an energy carrier in low-carbon energy systems, as it can be produced using renewable electricity in an electrolyser. Especially, its value for long-term energy storage is emphasized due to its high gravimetric energy density, low cost per kWh stored and widespread availability of water. Also, its value for hard-to-abate sectors is emphasized: hydrogen can be used for refuelling of Fuel Cell Electric Vehicles (FCEVs), green steel making, as base for the chemical sector, for production of synthetic fuels, etc.

Low-carbon hydrogen is produced by an electrolyser, which converts electricity and water into hydrogen and oxygen. Typically produced at 30 bar pressure, the hydrogen is often further compressed to increase energy density and reach the required pressure level for the intended application. The hydrogen is then stored in carbon fibre or steel pressure tanks or underground salt caverns. Finally, the hydrogen can be used for refuelling of FCEVs, green steel making, as base for the chemical sector, for production of synthetic fuels, etc. Alternatively, hydrogen can be reconverted into electricity, in which case hydrogen merely acts as energy storage. This conversion happens in a fuel cell, which converts hydrogen and oxygen (from the air) into water and electricity. Whereas a Power-to-Hydrogen (P2H) system can only provide flexibility on the demand side, a Power-to-Hydrogen-to-Power (P2H2P) system with re-conversion of hydrogen into electricity can provide flexibility both on the demand and supply side of the electric grid.

Several examples projects using hydrogen have taken place. In the Netherlands, more than 160 hydrogen-related projects are underway, with a focus on [30]. In Brütten, Switzerland, an apartment building is

independent of grid electricity year-round due to a P2H2P system [37]. The research institute Eidgenössische Materialprüfungs- und Forschungsanstalt (EMPA) in Dübendorf, Switzerland, has a future mobility demonstrator called MOVE, which includes an electrolyser and hydrogen refuelling station (Fig. 2.1).

1.2.1 Flexibility of electrolysers

In this section, special attention is brought to the electrolysers, as they are a central component in both P2H and P2H2P systems. An electrolyser is a device that converts water and electricity into hydrogen and oxygen. Its main component is the stack of electrolysis cells connected in series. When a DC voltage is set over an electrolysis cell, current will flow through the cell and hydrogen will be produced. A higher voltage will lead to more current and therefore, more hydrogen. The electrolyser load can thus be regulated by adjusting the voltage on the stack.

Next to the stack, the electrolyser includes auxiliary systems like the power supply, water deionization system, water circulation and oxygen management system, hydrogen gas drying and cleaning systems, cooling system and control system also called Balance of Plant (BoP). At higher loads, there are more losses in the stack which leads to inefficiency. But at lower loads, the BoP takes a relatively large amount of power. Therefore, the loads in the middle of the range are most efficient.

There are three main water electrolysis stack types: Proton Exchange Membrane or Polymer Electrolyte Membrane (PEM), alkaline, and solid oxide. Since PEM has been identified as most suitable for flexible operation [6] and the MOVE electrolyser is also of type PEM, only PEM will be considered in this thesis.

The electrolyte in the stack has to be at a certain temperature for efficient hydrogen production to take place and several processes have to ensure safety of the hydrogen gas before production begins. Therefore, PEM electrolysers often distinguish between an off mode, standby mode and on mode. A cold start is a transition from off to on and can take up to 10 minutes for PEM electrolysers [6]. A hot start is the transition between standby and on mode and can happen in less than 10 seconds since in standby the system is kept under pressure at the right temperature. Electrolysers are subject to degradation and there have been concerns that flexible operation can accelerate degradation. Other studies suggest however that flexible operation does not negatively affect the degradation rate if executed properly or could even slow down degradation [6]. The research is not conclusive. Therefore, degradation effects are ignored in the rest of this thesis. Flexible operation without unreasonable degradation has been demonstrated.

Furthermore, PEM electrolysers can be ramped within one second from 0 to 100% of their range [6]. These results suggest that electrolysers are indeed suitable for flexible operation. For PCR and aFFR services, the electrolyser needs to be in standby mode, while for mFFR the electrolyser can also be turned off. Several studies confirm the fast dynamics of PEM electrolysers. In [33], a PEM electrolyser passes the test to participate in PCR. PEM electrolysers are even suggested for virtual inertia (replacement of rotational inertia in traditional energy systems)[13]. [2] suggests electrolysers for voltage control. Since literature agrees on the fact that electrolysers are technically capable of providing flexibility, the more interesting question to ask is whether this is economically and sustainably viable and how the flexible operation is best realised.

1.2.2 Literature review on flexible control of Power-to-Hydrogen(-to-Power) systems

Due to the potential of hydrogen and the flexible capabilities of electrolysers, many studies have been done on their operation and economic feasibility.

50+ studies from recent years looking into the flexible operation of electrolysers were identified. Many contexts and systems are considered, such as PV, wind [39], connection to industrial processes, hydrogen refuelling [42], combination with battery, microgrid, electrical grid, hydrogen grid, with fuel cell, with building(s), with different sizes of storages. While some studies use measurements, most studies use a model of the system. Models range from very simple to very detailed and include context systems such as wind turbines and PV. Some studies assess the system based on a rule-based control, while most perform a deterministic optimization on the system and some even make and test an actual control algorithm to operate the system (some with real experiments). Mixed-Integer Linear Program (MILP) is the most common algorithm for optimization and control. Depending on the study, the system participates in the electricity and/or balancing market, or is off-grid. Nearly all studies have economical performance indicators.

The studies unanimously agree that the flexible operation of electrolyser increases profitability compared to non-flexible operation [28] [17]. [31] reports that electrolyzers are more profitable under real-time pricing than under fixed pricing, suggesting that they make a positive contribution to the flexibility of the electricity grid. [39] finds that the steady state operation of electrolyzers using batteries is not optimal, and that it is preferred to meet a hydrogen demand than to convert hydrogen back into electricity using a fuel cell.

The studies that discuss the balancing market agree that participation in the balancing market additionally to the day-ahead market improves profitability. [35] mentions improvement in profitability from participation in ancillary services. However, the capital costs of the system are high and the profits might or might not compensate for the capital cost [17]

There are also some things missing from the studies. The heat output of electrolyzers and fuel cells is rarely considered as a valuable energy source. Most studies assess the system based on an economic indicator, except [41], who reports decreased CO₂ emission because of flexible operation. Also, while many studies do economical assessment they fail to draw generalizable conclusions about flexibility. If flexibility indicators are used, these are often very specific and not universal/holistic.

Model accuracy is another big challenge in the literature. The very detailed models in some studies cannot be used in practise for control because of long computation time. Moreover, some of these detailed models still ignore energy use by auxiliary systems and startup behaviour, which have a large effect on flexibility in reality [6] [24]. Simplified models ignore these behaviours altogether, which can lead to false conclusions. Furthermore, most studies optimize with a maximum horizon of one or two days. The long term is ignored, even though hydrogen has been identified as a candidate for long term energy storage. Taking into account both a short and long term horizon is a big challenge.

1.3 Control of flexible energy systems

Model Predictive Control (MPC) is a technique that can be used for the flexible control of energy systems. In MPC, a model of the system and predictions of future disturbances as well as electricity prices are used to calculate the optimal input plan for a certain prediction horizon while satisfying constraints. The first control input of that plan is then applied to the energy system. In the next timestep, the current system state is updated with measurements and the disturbance predictions are updated as well. Again, the optimal input plan is calculated, etc. etc. The optimization is often done using a Mixed-Integer Linear Program (MILP) scheme and is of the general form (fully explained in Eq. 3.1):

$$\begin{aligned}
u_t = \arg \min_{u_t} \quad & \sum_{t=1}^T C(u_t) \\
\text{s.t.} \quad & x_{t+1} = T(x_t, u_t, d_t) \quad \forall t \in \{1, \dots, T\} \\
& u_t \in U, x_t \in X, x_{T+1} \in X \quad \forall t \in \{1, \dots, T\} \\
& x_1, U, X, d_t \quad \text{given}
\end{aligned} \tag{1.3}$$

MPC problems are typically limited to prediction horizons of a few days due to the intensive computational power needed to solve the underlying optimization problems. However, as previously discussed, hydrogen can both be used for short-term flexibility and seasonal energy storage hydrogen systems excel at longer-term energy storage. Limiting the prediction horizon to a few days can severely underutilize the long-term storage capacities of the system. To include a longer horizon, Often, this is solved by adding a terminal cost or value function at the end of the MPC optimization, resulting in the following general formulation (fully explained in Eq. 3.1):

$$\begin{aligned}
u_t = \arg \min_{u_t} \quad & \sum_{t=1}^T C(u_t) + V_{T+1}(x_{T+1}) \\
\text{s.t.} \quad & x_{t+1} = T(x_t, u_t, d_t) \quad \forall t \in \{1, \dots, T\} \\
& u_t \in U, x_t \in X, x_{T+1} \in X \quad \forall t \in \{1, \dots, T\} \\
& x_1, U, X, d_t \quad \text{given}
\end{aligned} \tag{1.4}$$

where $V(x_T)$ represents the future cost as a function of the last state variable of the prediction horizon. The other way round, it can be seen of the value of the energy in the storage. However, determining the value function (or the value of the hydrogen in storage) is non-trivial. Considering a system with PV and electricity prices, the value (or avoided cost, or terminal cost function) depends on the PV power and electricity prices, device efficiency, etc. etc. in future timesteps. Already mention MOVE system. A standard method for obtaining this function is missing. Attempts at determining the value function are further described in Chapter 3.

Hydropower systems have been used for a long time for both short-time flexibility provision and long-term energy storage. Can we learn from control algorithms for hydropower systems? In 1991, Pereira and Pinto developed the Stochastic Dual Dynamic Programming (SDDP) algorithm for hydropower scheduling [32]. As the name suggests, it uses principles from stochastic, dual and dynamic programming. The algorithm has the ability to handle stochastic problems with multiple sequential reservoirs and long time horizons. The algorithm has been popular for hydropower scheduling since. This is exactly what we need for optimizing our hydrogen system!

In this thesis, MPC and SDDP are combined, where the MPC handles optimization over the short term horizon while SDDP establishes the value function to take into account the long term horizon. The exact details and solution logic and further literature review is addressed in Chapter 3. Mention model "tricks".

1.4 Thesis outlook

1.4.1 Research gap and objectives

From the literature research, it is already clear that electrolyzers and Power-to-Hydrogen(-to-Power) systems are flexible from the seconds to seasonal timescale. It is also clear that flexible operation increases profitability. However, common and consistent indicators for flexibility are lacking. Waste heat is rarely considered as a valuable energy stream and non-economical objectives are rarely evaluated. Most importantly, control methods often fail to take into account longer timescales, from anywhere longer than a week up to seasonal timescales. This is a major limitation since Power-to-Hydrogen(-to-Hydrogen) systems are very suitable for providing long-term flexibility.

Therefore, the focus of this thesis is to find a flexible control method that can take into account short and mid-term timescales (<week) *and* long-term timescales (>week). The method should be usable in real time. The following research goals are identified to achieve this goal:

1. To create a model of a Power-to-Hydrogen system which is accurate enough to capture the intricacies and limitations of flexible operation yet simple enough to be used for realtime control.
2. To propose a flexible control algorithm that takes into account timescales from one hour all the way to seasonal. *Flexibility for Energy* is optimized under day-ahead electricity prices.
3. To assess the short-term flexibility potential of the Power-to-Hydrogen system, which can be offered for balancing power, and communicate this potential with system operators. The goal here is to optimize *Flexibility for Power*

1.4.2 Research Methods and Thesis structure

The rest of the thesis is structured as follows:

Chapter 2: Model A model of the right detail level is created using data from MOVE, a future mobility demonstrator at the research institute Eidgenössische Materialprüfungs- und Forschungsanstalt (EMPA) in Dübendorf, Switzerland. MOVE is a hydrogen refueling station with on-site hydrogen production from PV and electrolyser (Fig. 2.1). MOVE is then used as a further case study for control and flexibility assessment.

Chapter 3: Control Algorithm Discusses the control algorithm that takes into account multiple timescales. Stochastic Dual Dynamic Programming (SDDP)[32] is used to take into account timescales longer than a week. Model Predictive Control (MPC) is used to take into account timescales from an hour to one week. The correction of control signals after optimization allows to model the startup period of the electrolyser.

Chapter 4: Flexibility envelope The short-term *Flexibility for Power* potential is assessed and communicated using the concept of the *Flexibility envelope* [16]. The flexibility envelope is calculated with optimization of the system under worst-case scenarios.

Chapter 5: Conclusion and Discussion Conclusion, limitations and outlook on future work.

Table 1.1: Overview of flexibility types, timescales and methods addressed in this thesis and their corresponding sections in the thesis.

Section	Flexibility type	Timescale	Method
2	all	all	Model identification using historical data
3.1-3.3	Flexibility for Energy	>7 days	DDP, SDDP
3.4	Flexibility for Energy	1 hour - 7 days	MPC
3.4.1	Flexibility for Energy	<1 hour	Correction of control signals
4	Flexibility for Power	<24 hours	Flexibility envelope

Chapter 2

Model

The goal of this chapter is to create a model of a Power-to-Hydrogen(-to-Power) system that can be used for the flexibility assessment and the proposal of a control algorithm to achieve that flexibility. Specifically, it describes a model of MOVE, the future mobility demonstrator at EMPA. This section describes the model by devoting a section to each component.

MOVE (Fig. 2.1) is a refuelling station for hydrogen vehicles, which produces its own hydrogen. The main component is the electrolyser, which converts electricity and water into hydrogen and oxygen. The electrolyser is powered with AC power, partly from PV panels and partly from the electric grid. Two compressors increase the pressure of the hydrogen to achieve higher energy density for storage and so that it can be used in the 700 bar refuelling station. Pressure tanks store the hydrogen at different pressure levels. The 350 bar refuelling station is not modelled, because it is used infrequently. As a result, the usable pressure range of the 440 bar tanks is increased, but 350 bar refuelling is not guaranteed anymore. The neighbouring NEST building is a modular research and innovation building with several functions. It is connected to the same electricity and heat network.

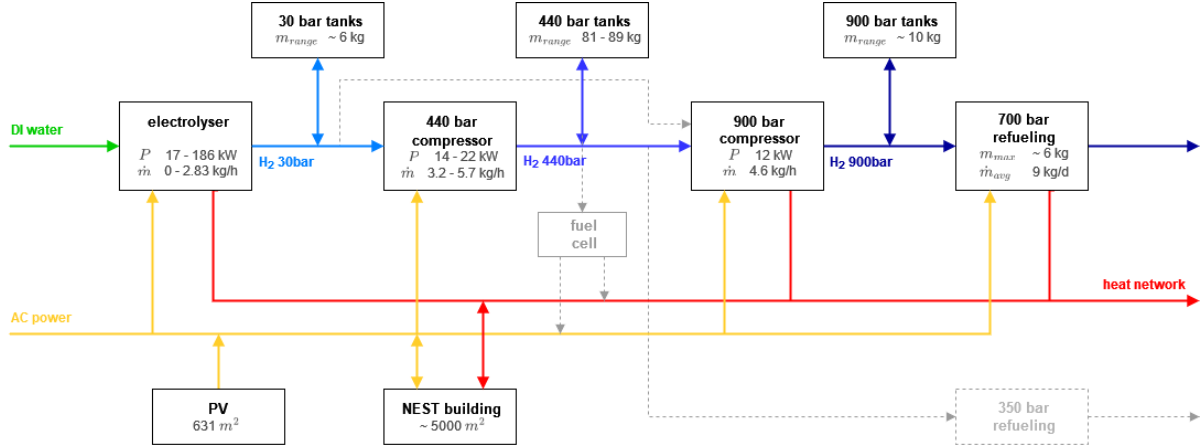


Figure 2.1: Schematic overview of MOVE. For simplicity, several components are not shown: the battery trailer, EV charging station and CNG fueling station, since they are not relevant for this thesis; the HCNG fueling station, since it is only used for one experimental vehicle. A fuel cell is not present in move, but modelled as a virtual technology.

MOVE is an excellent representation of a small-scale multi-energy energy community, as it includes in-house electricity and hydrogen production, a hydrogen demand and heat and electricity demand from a building. Numerous sensors collect data from MOVE, which are available from December 2017 on a minute resolution. These data are used to build the model. It should be noted that the data has many errors and is not always well documented, which makes model identification a very time-intensive process. Still, the use of a case study is valuable since it allows for model verification and potential future experiments.

Three different models are created: (i) the main model, a Mixed-Integer Linear Program (MILP) with

an hourly resolution, used for the short-term optimization with MPC and flexibility assessment; (ii) an Linear Program (LP) version of the model, used to optimize the long term horizon with SDDP; and (iii) a more precise non-linear model to simulate the system. Wherever the latter two deviate from the main MILP model, it will be clearly stated.

2.1 Hydrogen pressure, temperature and density

The mass of a fixed amount of hydrogen always remains constant, while pressure and temperature may change subject to a nonlinear relationship. Mass-based models are therefore the simplest. For this reason, *mass and mass flow rate are used in this thesis to quantify hydrogen amount and flow.*

Like any gas, hydrogen has a fixed relationship between pressure P , temperature T and density ρ . This relationship can be approximated with the ideal gas law:

$$\rho = \frac{P}{RT} \quad (2.1)$$

where R is the gas constant for hydrogen ($4.124 \text{ kJ kg}^{-1} \text{ K}^{-1}$). However, the ideal gas law is not sufficiently accurate for hydrogen pressures greater than 40 bar. For real gases, the ideal gas law is extended to

$$\rho = \frac{P}{ZRT} \quad (2.2)$$

where Z is a unitless compressibility factor that depends on pressure, temperature and gas species. Lemmon et al. [26] developed an equation for the compressibility factor of hydrogen:

$$Z(P, T) = 1 + \sum_{i=1}^9 a_i \left(\frac{100[K]}{T} \right)^{b_i} \left(\frac{P}{1[MPa]} \right)^{c_i} \quad (2.3)$$

where a_i , b_i and c_i are constants. The combination of equations 2.2 and 2.3, further referred to as Lemmon equation, estimates hydrogen density with an uncertainty of 0.04% (coverage factor of 2) in the temperature range of 250-400K for pressures up to 1200 bar. The Lemmon equation is used in the rest of this thesis to convert between hydrogen mass, pressure, temperature and volume.

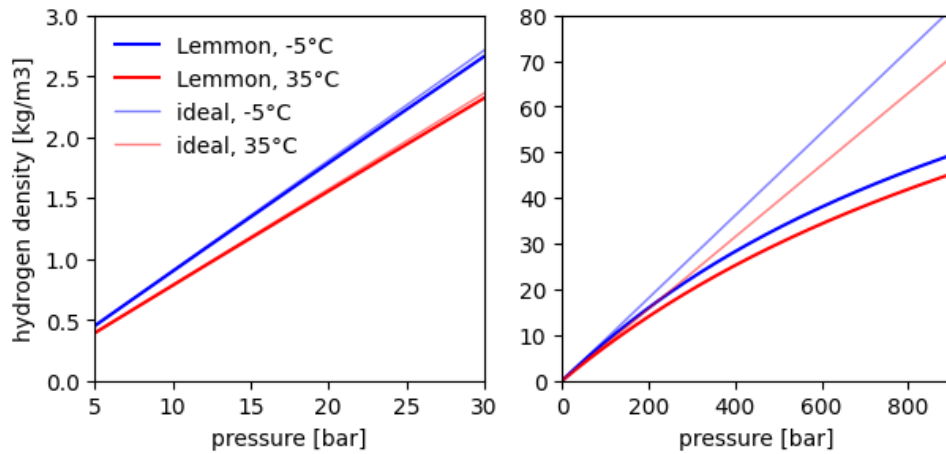


Figure 2.2: Comparison of ideal gas law and Lemmon equation. The right figure shows the pressure range of all tanks while the left graph is a zoom-in on the pressure range of the 30 bar tank. The line color represents different temperatures. Opaque lines represent the Lemmon equation while more transparent lines represent the ideal gas law.

2.2 Electrolyser

Following up on section 1.2.1, which discussed electrolyzers in general, this section describes a model of the specific electrolyser in MOVE (Fig. 2.3). It is a PEM electrolyser of the model Hogen C30

produced by Proton OnSite and it was installed in 2015. It has a maximum capacity of 186 kW and 2.83 kg h^{-1} of hydrogen, which is produced at 30 bar pressure. The electrolyser has 3 stacks, each with 65 electrochemical cells.

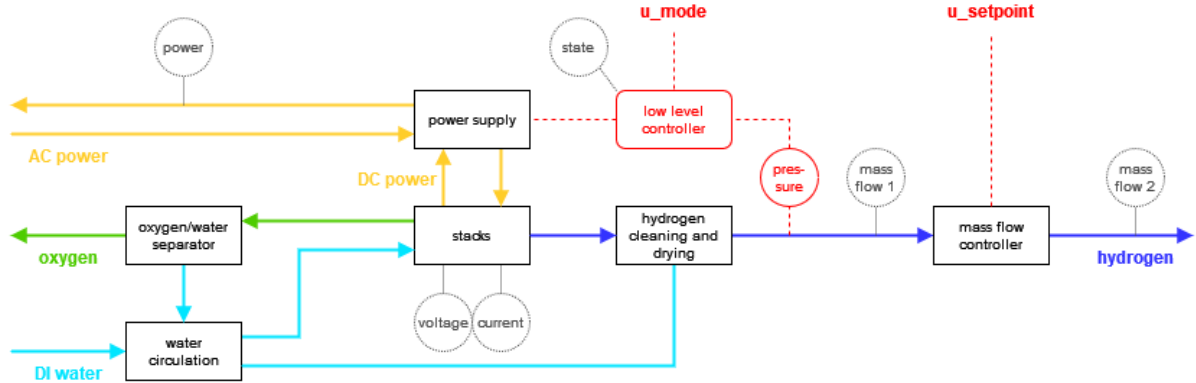


Figure 2.3: Simplified representation of the electrolyser in MOVE. It shows the subsystems, the control system and the most relevant sensors. Most subsystems also have a cooling system and a power supply, which are not shown for the sake of readability. Oxygen is emitted into the environment.

Unlike many electrolyzers, the stack voltages and currents of the MOVE electrolyser cannot be controlled directly. Instead, the on/off state and the mass flow rate are controllable. The mass flow controller is located at the hydrogen output. A pressure sensor is placed just before the mass flow controller. The low-level controller of the electrolyser is designed to always keep the hydrogen output pressure at a setpoint of 30.5 bar. If the setpoint of the mass flow controller is increased, the valve opens and more hydrogen flows through it. Consequently, the pressure at the pressure sensor is decreased, which triggers the low-level controller to increase the stack currents. This causes more hydrogen production and restores the hydrogen output pressure to the setpoint value.

It should be noted that there are two hydrogen mass flow meters: one at the electrolyser side of the mass flow controller (\dot{m}_{del}) and one at the buffer side of the mass flow controller (\dot{m}_{buf}). The two meters give significantly different readings. \dot{m}_{del} oscillates in sync with the electrolyser power, while \dot{m}_{buf} is more smooth (Fig. 2.4). At low mass flow, \dot{m}_{buf} is less than \dot{m}_{del} . At high mass flow, \dot{m}_{buf} is greater than \dot{m}_{del} (Fig. 2.5). A comparison of the electrolyser mass flow to the change of hydrogen mass in the 30 bar tanks suggests that \dot{m}_{buf} is more accurate. This is confirmed by specification sheets from the manufacturer. \dot{m}_{buf} is therefore accepted as ground truth.

The electrolyser has an efficiency of around 60%. The rest of the energy is released as heat. Therefore, the electrolyser is cooled with a cooling system, and this cooling system provides heat to the heat network at EMPA. Electrolyser waste heat is a valuable energy stream [22]. However, there are no measurements of the stack temperature and the measurements of the electrolyser cooling system are extremely limited. This makes identification of the usable heat output impossible. The heat aspect is only shortly addressed in Chapter 4.

2.2.1 Transient behaviour

The electrolyser can be in three different mode: on, standby and off. In standby, the electrolyser is kept at the right temperature and pressure but does not produce hydrogen. The transition from off to on is called cold start-up and the transition from standby to on is called warm start-up. Fig. 2.4 shows the power and mass flow of the electrolyser during cold start-up, normal operation and shutdown.

When the electrolyser is in on or standby mode, the power and mass flow oscillate around the setpoint with a short period of around 2 minutes and a long period of around 20 minutes [23]. The reason for these oscillation cannot be identified because the exact behaviour of the low-level controller and the mass flow controller are not known and stack temperature measurements are missing. Therefore, the oscillations are further ignored and rolling averages are used for system identification.

The reaction time for shutdown and load ramping is very fast. Reaction delays were neither observed in the minute-resolution data, nor by Laaksonlaita [23]. The observation corresponds to the literature (Sec. 1.2.1), which emphasizes the fast dynamics of PEM electrolyzers as long as they are at the right

temperature and pressure. Therefore, the electrolyser is modeled as a static model in the on and standby mode.

However, cold start-up takes around 7 minutes, which is again in line with the literature (Sec. 1.2.1). This start-up period consists of two sub-periods: In the first period of 257 seconds on average, the electrolyser goes through a few startup processes that each correspond to a discrete power level. In the second period, the electrolyser ramps up production to the desired level. This period lasts 30 s-3.5 min dependent on the setpoint. In the MILP the startup is modeled as 6 minutes of a constant startup power $P^{startup}$ and then full production is reached immediately (Fig. 2.4. In the LP model, the startup period is omitted.

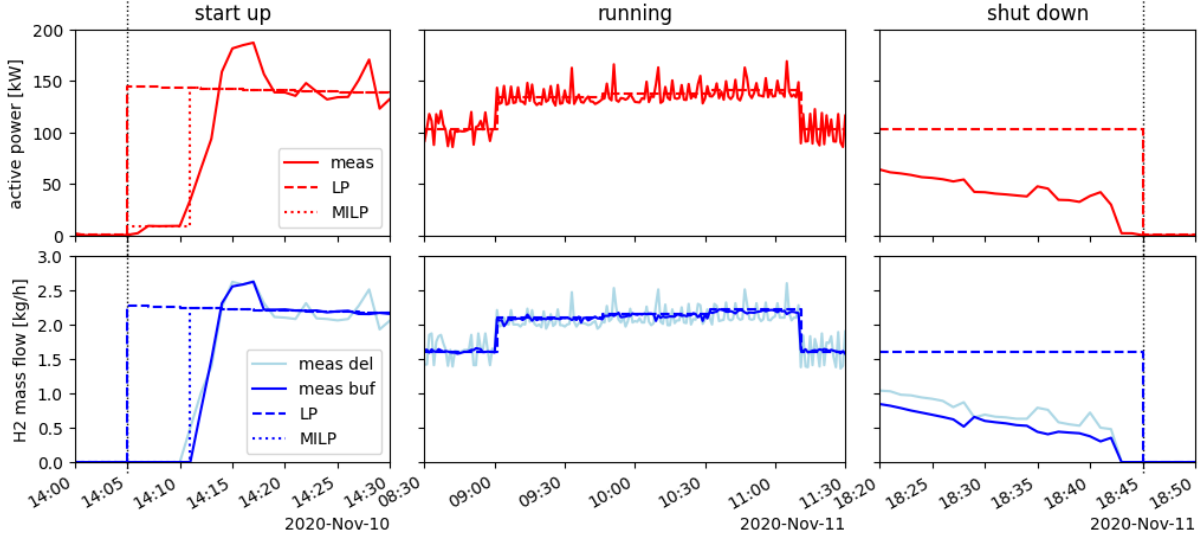


Figure 2.4: Electrolyser behaviour in time and model equivalents. Although the shutdown is normally immediate, this specific case shows a shutdown due to high pressure in the 30 bar buffer.

2.2.2 Control of mass flow

The mass flow is controlled by the setpoint (0-100%) specified in the mass flow controller. Since the relationship is mostly linear, a mapping between the two values can be constructed using linear least-squares regression:

$$\dot{m}^{el} = 3.047 \cdot u^{sp} - 0.219 \quad (2.4)$$

where \dot{m}^{el} is the hydrogen mass flow of the electrolyser in kg h^{-1} and u^{sp} is the setpoint (0-100%). The data shows systematic deviations from the linear fit in certain setpoint regions (Fig. 2.5a). These inaccuracies do not pose a problem, since simulations rather than experiments are conducted in this thesis. The direct mapping between setpoint and mass flow allows to only utilize mass flow for the optimization and simulation process, while the setpoint is calculated in the post-processing phase. In short, the setpoint is merely used as indicator instead of actual control input. Of course, the mapping should be improved before running any experiments on the real system in subsequent research. Even then, the mapping can be arbitrarily complex, as it will not occur in the optimization problem.

When the pressure differential between the electrolyser and the connected 30 bar tanks (buffer) gets small, a mass transport limit comes into place, constraining the mass flow to a certain maximum. The exact nature of this limit is very specific to the MOVE system. Other electrolyser systems have different flow resistance or might even circumvent the issue by increasing the outlet pressure. Fig 2.5b shows that at 100% load, the limit overrides the setpoint when the buffer pressure is greater than 20 bar.

To establish a relationship between the mass flow limit and buffer pressure, datapoints where the electrolyser is running regularly at 100% load and the buffer pressure is above 20 bar are selected. A piecewise linear curve with 4 segments is fitted to these data using least-squares regression (Fig. 2.5b). However, conversion from mass to pressure is needed to use the constraint in optimization and simulation. Unfortunately, the Lemmon equation is too complex to use in an optimization model. Therefore, the Lemmon equation is linearized in the relevant region from -2.5 - 33.5°C and 20-30bar, resulting in

$$p = f_{\text{lemmon}, \text{lin}}(m) = \frac{3590.8}{(309.3 - T) \cdot V} \cdot m - \frac{116.0 - 0.59 \cdot T}{309.3 - T} \quad (2.5)$$

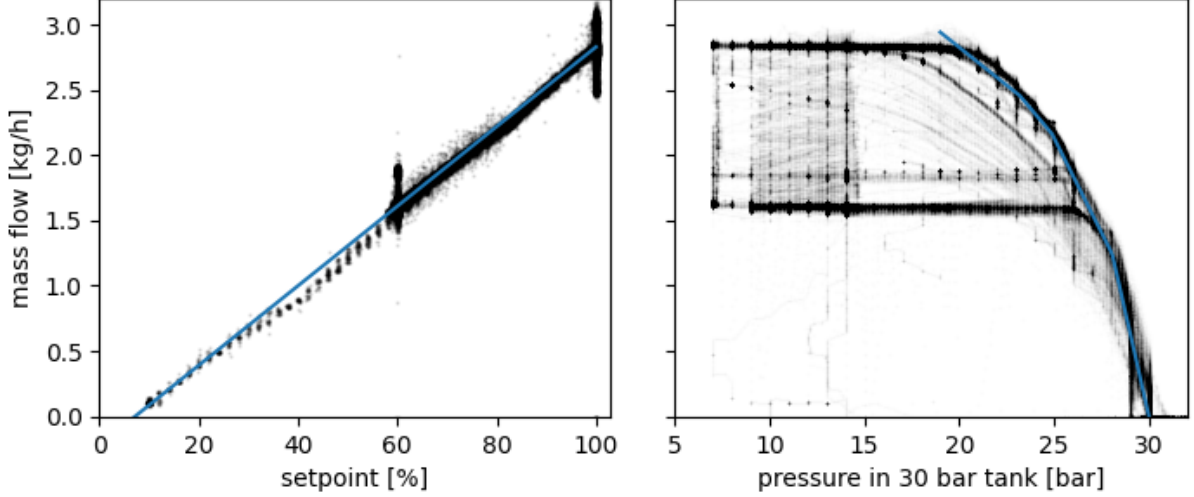


Figure 2.5: Relationships for the control of electrolyser mass flow. The underlying data is shown in black while the fitted curves are shown in blue.

where $m(\text{kg})$ is the hydrogen mass, $T(^{\circ}\text{C})$ is the tank temperature, $V(\text{m}^3)$ is the tank volume and $p(\text{bar})$ is the pressure. Note that the relationship is linear in the optimization problem because T and V are known beforehand. This then allows to formulate the mass transport constraint

$$\dot{m}^{el} \leq f_{el,mtx} (m^{st,low}, T^{st}) \quad (2.6)$$

where \dot{m}^{el} is the electrolyser mass flow and $f_{el,mtx}$ is the fitted piecewise-linear curve.

2.2.3 Relationship between mass flow and power

Next, an equation for the power consumption of the electrolyser should be established. Outside of the start-up process, the power is mainly dependent on mass flow. It might be that the power is also influenced by the stack temperature, but this cannot be identified as no measurements are available. The power oscillates in sync with mass flow \dot{m}_{del} and the relationship between them has low spread (Fig. 2.6). Two curves are fitted through these datapoints using least-squared regression: a piecewise linear curve for the MILP model and a two-degree polynomial for the simulation model. Then, a linear line is fitted through \dot{m}_{del} and \dot{m}_{buf} , which shows more spread. The two curves added together define the relationship between mass flow and buffer, resulting in

$$P^{el} = f_{el} (\dot{m}^{el}) \quad (2.7)$$

where f_{el} is piecewise-affine in the MILP model and a two-degree polynomial in the simulation model.

At zero mass flow, the electrolyser is in standby modus with a power consumption of 16.7 kW. This is a very high consumption compared to the average power when the electrolyser is turned on, 0.64 kW. Therefore, it is important to model the on and off state separately using a binary variable. This implementation is further discussed in Section 3.4.

This relationship can be translated into efficiency values. It is important to specify whether the efficiency is defined relative to the Higher Heating Value (HHV) or Lower Heating Value (LHV) of hydrogen. These describe the energy content of hydrogen with either water or steam as end product respectively. HHV ($=39.4 \text{ kW h kg}^{-1}$) is used in this thesis since the electrolyser takes water as input. Electrolyser efficiency can be split into three parts: (i) auxiliary efficiency, which describes the power needs of auxiliary systems; (ii) voltage efficiency, which describes irreversibilities in the stack; and (iii) Faraday efficiency, which describes hydrogen permeating through the PEM membrane and other hydrogen losses in the system. Summed up, they form the system efficiency. Fig. 2.7 shows the different efficiencies of the MOVE electrolyser. The electrolyser reaches a maximum efficiency of 61.74% ($63.82 \text{ kW h kg}^{-1}$) at a setpoint of 68%. At low loads, efficiency is low because of relatively high power use of auxiliary systems. At high loads, efficiency is lower due to increased irreversibilities in the stack.

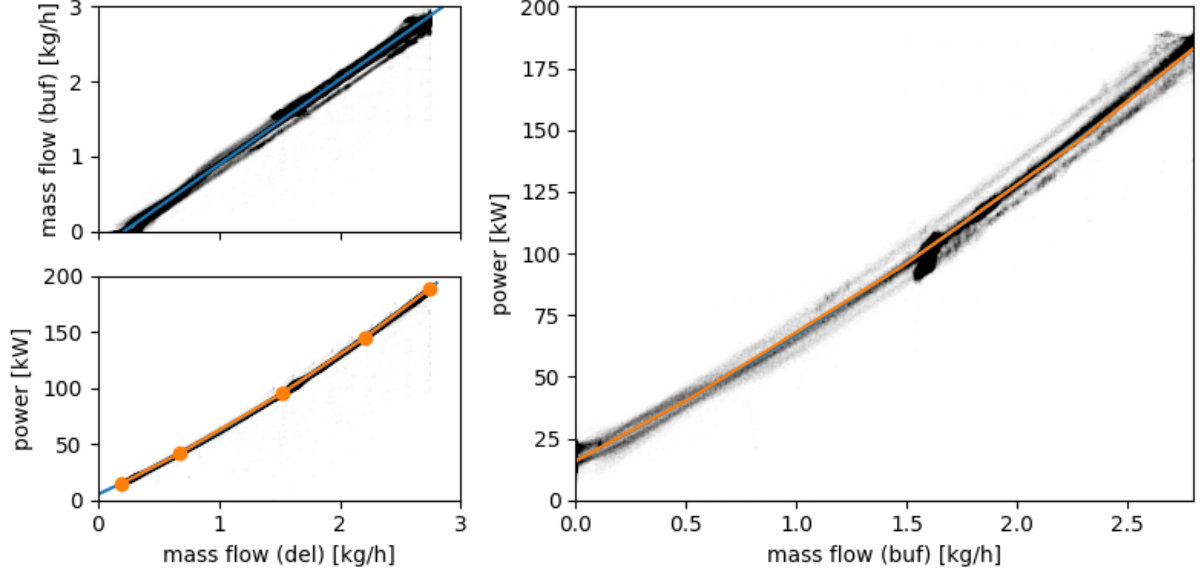


Figure 2.6: Relationship between mass flow and power of the electrolyser. The underlying data is shown in black while the fitted curves for the MILP optimization model are shown in color. The relationship in the right graph is the combination of the two relationships in the graphs on the left.

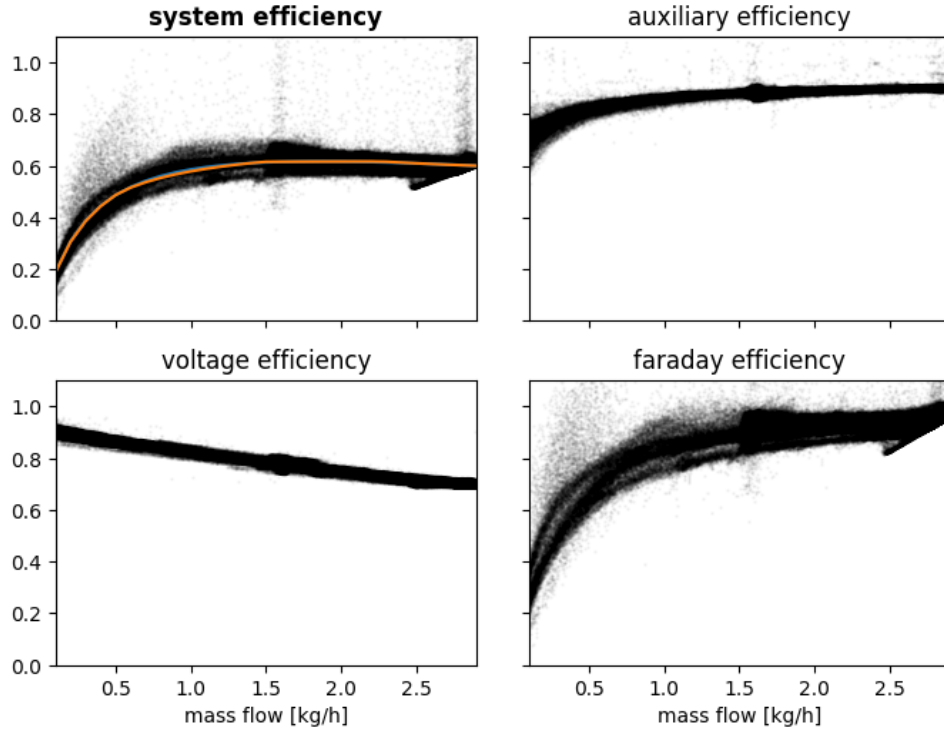


Figure 2.7: HHV efficiency of MOVE electrolyser. The underlying data is shown in black while the orange line shows the efficiency according to the piecewise-linear mass flow to power relationship (Eq. 2.7). The meaning of auxiliary, voltage and Faraday efficiency are explained by Eq. 2.8-2.10

$$\eta_{aux} = \frac{\text{stack power}}{\text{total electrolyser power}} \quad (2.8)$$

$$\eta_{vol} = \frac{\text{stack voltage}}{\text{thermoneutral voltage}} \quad (2.9)$$

$$\eta_{far} = \frac{\text{actual hydrogen production}}{\text{theoretical hydrogen production in stack}} \quad (2.10)$$

2.3 Hydrogen storage tanks

MOVE stores hydrogen in carbon fibre tanks at three different pressure levels as shown in Fig. 2.1. The tanks have pressure and temperature sensors, whose measurements can be used to determine the mass of stored hydrogen.

The storage limits of the tanks are determined by the maximum pressure that the tanks can withstand. However, the pressure requirements of the compressors and the electrolyser are more constraining, so that exceeding the safety limits of the tanks is impossible. The most accurate model would therefore not implement storage constraints but disable operation of the compressors when the pressure requirements are exceeded. However, such a model would require extra binary variables, which negatively impacts solve time. In this thesis, storage constraints based on the pressure requirements of the electrolyser and compressors are implemented instead. This slightly reduces the usable range of the tanks, since the tanks are not allowed to exceed the pressure requirements when the temperature changes.

To convert the pressure requirements into mass constraints, the temperature of the tanks needs to be known. Since the tanks are located in a non-heated building, their temperatures follow a smoothed and shifted version of the ambient temperature (Fig. 2.8). The tank temperatures are between $-2.5\text{ }^{\circ}\text{C}$ and $33.5\text{ }^{\circ}\text{C}$ for at least 99% of the time. A detailed auto-regressive prediction model for the tank temperatures was already identified by Laaksonlaita [23]. He shows that the tank temperatures are strongly dependent on the ambient temperature and weakly dependent on solar irradiation, pressure changes and incoming hydrogen, the latter three of which can be ignored in models. This means that the tank temperatures are not significantly influenced by the operation of the system, so that they can be modeled as disturbances. In this thesis, historical temperature measurements are used as deterministic input to the MPC. These measurements, which are rounded to integer values, are grouped and averaged over a rolling window to form one single temperature value for all tanks. The choice for a deterministic optimization is made because temperature prediction inaccuracies of a few degrees Celsius would only cause small inaccuracies in the storage tank constraints. Table 2.1 gives an overview of the storage constraints.

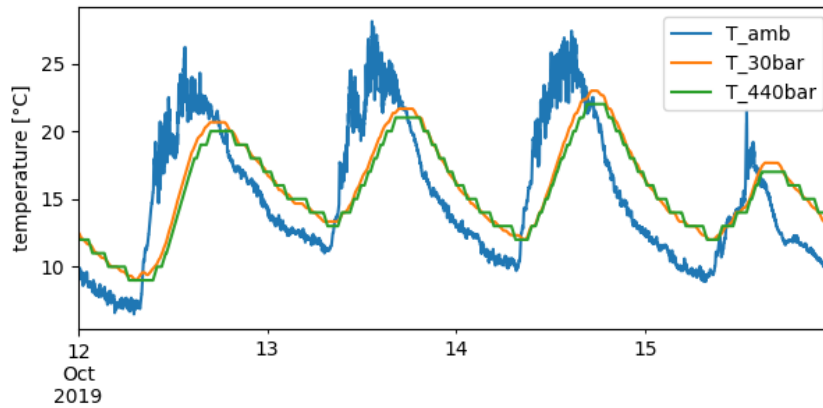


Figure 2.8: Buffer temperature

Table 2.1: Properties of the storage tanks

	volume [m ³]	min. pressure [bar]	max. pressure [bar]	mass capacity at -2.5 degC [kg]	mass capacity at 33.5 degC [kg]
30 bar	3.186	7	30	6.4 (2.0 - 8.4)	5.7 (1.8 - 7.4)
440 bar	3.186	25	440	89.2 (7.0 - 96.2)	80.8 (6.2 - 87.0)
900 bar, low/mid/high	0.5/0.25/0.25	550/640/730	890	10.4 (38.4 - 48.8)	10.0 (35.1 - 45.1)

The lower pressure limit of the 900 bar tanks is not determined by the compressor but rather by the remaining pressure after vehicle refuelling. Hydrogen needs a pressure gradient to flow, so the 900 bar tanks are divided into a low, middle and high bank which are used consecutively during refueling. First, the low bank fills the vehicle to a first pressure level, p.e. 360 bar. Then, the middle bank fills the vehicle to a second pressure level, p.e. 560 bar. Lastly, the high bank fills the vehicle to the target pressure level, i.e. 700 bar. This three-bank layout has a greater usable range than a single-bank layout, as it

can be partly emptied to below 700 bar. However, it is non-trivial to determine the exact lower pressure limits. These limits depend on many factors, such as temperature, tank volumes, start and end pressures of the vehicles, start pressure of the storage tanks, control system and minimum pressure differential. An attempt at theoretical determination of the lower limit was therefore unsuccessful. The data shows that at pressure levels of 550, 640 and 730 bar for the low, middle and high bank, the last refuelled car was still able to reach target pressure in most of the cases. Below these levels, cars are likely to not reach the target pressure. Therefore, these levels chosen to approximate the lower constraint for the 900 bar tanks. Interested readers are referred to [38] for more details regarding hydrogen refuelling stations.

2.4 Compressors

MOVE has two high pressure piston compressors. The 440 bar compressor moves hydrogen from the 30 bar tanks to the 440 bar tanks. The 900 bar compressor moves hydrogen from the 30 bar tanks and 440 bar tanks to the 900 bar tanks. There is little information available about the low-level controller of the compressors and for most of the period they run at a pre-set speed. Although it might be possible to change this pre-set speed, in this thesis it is simply assumed that they run at a pre-set speed and we can only turn the compressor on and off. Both compressors have a fast reaction time, with startup and shutdown in less than a minute.

Firstly, a model for the 900 bar compressor is identified. A rolling average is taken for the compressor power, since it strongly oscillates. For most of the analysed period, the compressor runs at a single speed. Periods with a different speed and moments with active hydrogen refuelling are removed from the data. Then, the mass flow can be calculated from mass differences in the 900 bar tanks. The hydrogen mass in the 900 bar tanks estimated with the Lemmon equation using pressure and temperature measurements. Since the 900 bar tanks have no temperature sensor, the average temperature of the 440 bar tanks is taken as proxy. Both mass flow and power seem normally distributed around a single value (Fig. 2.9a). No dependence on source- or target pressure is identified and the spread seems mostly due to oscillations. Therefore, the 900 bar compressor can be characterized by a single power and mass flow value (Table 2.2).

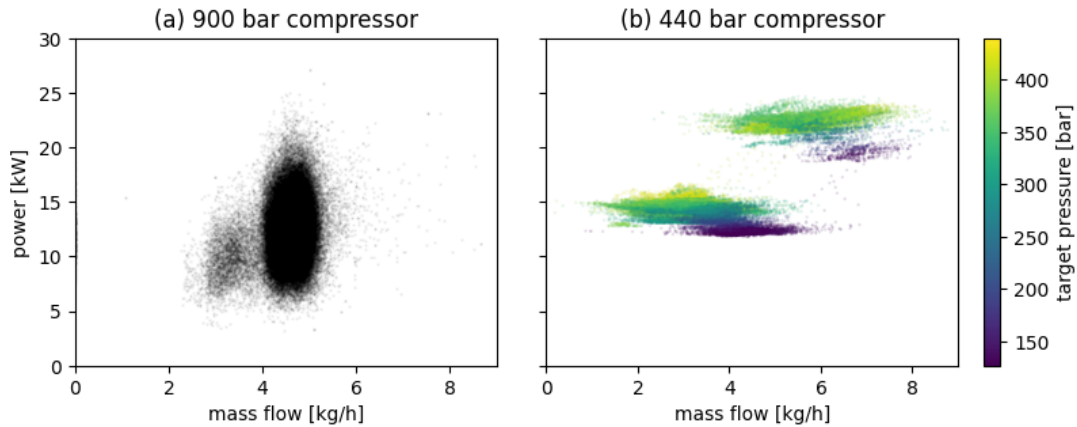


Figure 2.9: Power and mass flow of compressors.

Secondly, a model for the 440 bar compressor is identified. In the period from February 2020 until September 2021, the compressor often operates with lower-than-usual efficiency and the data is less consistent. It is assumed that the compressor had sub-optimal settings during this period, which is consequentially removed from the data. The mass flow is estimated from mass differences in the 440 bar tanks (calculated in a similar way to the 900 bar tanks) and corrected for hydrogen outflow due to 350 bar refuelling events and the 900 bar compressor.

It turns out that the 440 bar compressor can operate at two distinct speeds, dependent on the pressure in the 30 bar tank (Fig. 2.10left). The two speeds have distinct power and mass flow levels (Fig. 2.9b). Furthermore, the efficiency is strongly dependent on the target pressure, i.e. the pressure in the 440 bar tanks (Fig. 2.10). Modelling both pressure-dependencies in the optimization models is possible, but increases the interdependencies between state variable and operational variables, which negatively influences computational speed. Since the focus in this thesis is not on the compressors, it is chosen to

Table 2.2: Compressor information

	efficiency [kWh/kg]	average mass flow [kg/h]	average power [kW]	base load [kW]
900 bar compressor	2.724	4.551	12.424	0.027
440 bar compressor	4.078	4.448	18.138	0.395
— <i>high speed</i>	3.848	5.673	22.222	
— <i>low speed</i>	4.238	3.223	14.054	

simply take the average power and mass flow of both clusters. The resulting values are listed in Table 2.2. Note that these averages are biased towards high pressure regions of the 440 bar tanks, since the existing rule-based control system already turns on the compressor when the pressure drops below 350 bar, while we ignore 350 bar refuelling and therefore use the full range of the 440 bar tanks.

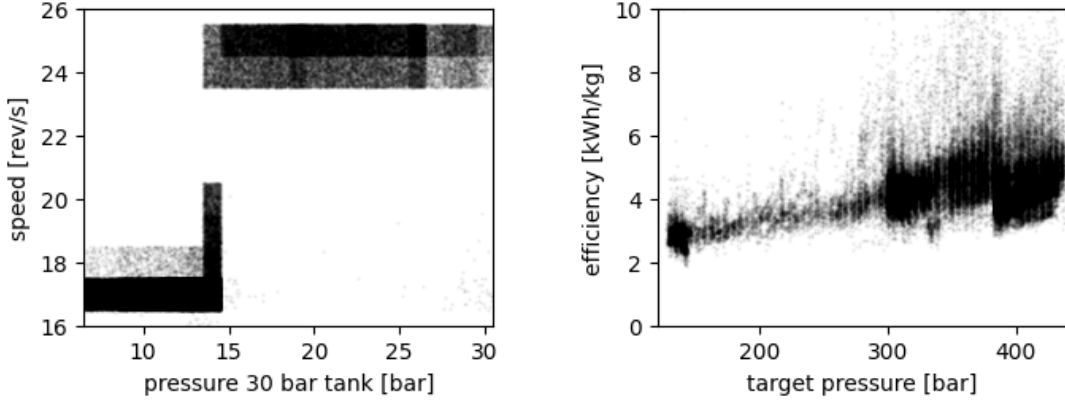


Figure 2.10: Details of the 440 bar compressor. Left: Two distinct compressor speeds based on the pressure in the 30 bar tanks. Right: Efficiency is strongly dependent on target pressure.

The aforementioned assumptions allow to model the compressor with two simple equations in the optimization model:

$$P_t^{comp440} = 4.078 \cdot \dot{m}_t^{comp440} + 0.395 \quad (2.11)$$

$$\dot{m}_t^{comp440} \leq 4.448 \quad (2.12)$$

Any mass flow below the maximum is interpreted as the compressor operating for only part of the timestep, which is a good assumption for sufficiently long timesteps. For example, a $\dot{m}_t^{comp440} = 2.224$ indicates that the compressor is on for half of the timestep. However, these constraints neglect any minimum operation time, which is realistic for such devices. This can be implemented by specifying a minimum massflow when turned on, however, this requires an extra binary variable which severely complicate the model. In this thesis, the minimum operation time is therefore ignored.

Concluding, there is room for improvement in the compressor models, taking into account minimum operation time and pressure dependencies. Since compressors are not the focus and we wanted an LP, these were not taken into account. However, it would be interesting to do a more detailed study on the compressors.

2.5 Hydrogen demand

In this section, a statistical model for the hydrogen refuelling demand at MOVE is constructed from refueling data between January 2017 and October 2022. The approach is similar to [23], with a few extensions. MOVE has two hydrogen dispensers for refuelling vehicles at 350 and 700 bar respectively. First, the data is cleaned, merging refuelling events that take place shortly after each other for the same customer and deleting refuelling events with less than 10 gram refuelled. The refuelling events usually last 3-5 minutes, but are simplified to happen in one minute, which greatly simplifies the analysis. This is a reasonable assumption as the number of users is low and it rarely happens that multiple cars refuel

within 5 minutes of each other. The 350 bar dispenser, meant for p.e. trucks and forklifts, is used for less than 7% of refuelled mass over the analysed period, with most 350 bar refuelling events taking place before August 2018. Therefore, 350 bar refuelling is further ignored.

2.5.1 Amount of refuelling events

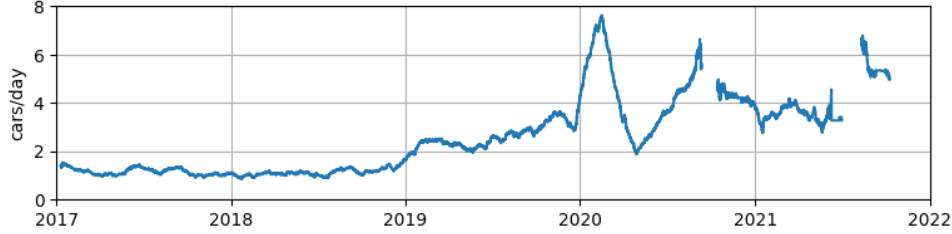


Figure 2.11: Average number of 700 bar refuelling events per day (centered rolling window of 8 weeks)

The 700 bar dispenser is mainly used for refuelling passenger cars. The average number of refuelled cars per day is not constant over the years (Fig. 2.11). A second observation is that considerably more cars refuel during work days (Mo-Fr) than during free days (Sa, Sun, holidays). For every week, the average daily car arrival rate for work days λ_w and for free days λ_f is plotted against the average daily rate λ_a for the entire week (Fig 2.12). It is found that this ratio is relatively constant, i.e. not affected by the weekly average. Through linear least-squares regression (excl. outlier points), the ratio $\frac{\lambda_w}{\lambda_a} = 1.187$ is found. Then, based on the average ratio of free days and work days per year, the ratio $\frac{\lambda_f}{\lambda_a} = 0.581$ is found.

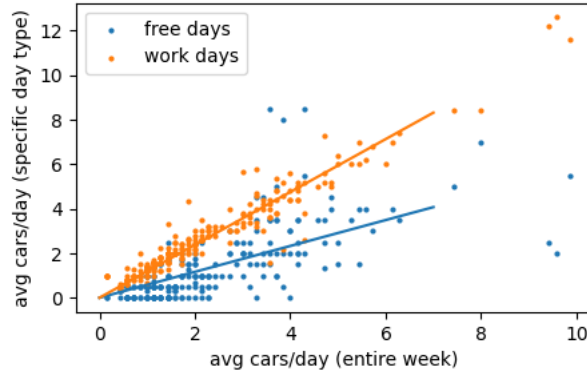


Figure 2.12: Relationship between the average number of cars per day during an entire week and the average number of cars during work/free days in the same week.

The hydrogen demand for mobility is assumed to be stagewise-independent. This means that the occurrence of a refuelling event does not influence the probability of refuelling events occurring in the future. This assumption is satisfactory when refuelling events last short and when the customer base is sufficiently large. The latter is dubious in MOVE, but assuming otherwise would lead to an overly complicated model. The Poisson distribution is a discrete probability distribution that describes how many events occur over a time period given an average occurrence rate. Under the assumption of stagewise-independence, it can describe the probability distribution for the amount of cars in a day given the average daily rate:

$$P_N(n) = \frac{\lambda^n}{n!} e^{-\lambda} \quad (2.13)$$

where n is the daily number of cars and λ is the average daily number of cars. Fig. 2.13 compares the data with results of the Poisson distribution for periods with a relatively constant daily arrival rate. Note that *the assumption of stagewise-independence means that the hydrogen demand cannot be predicted more accurately as time nears.*

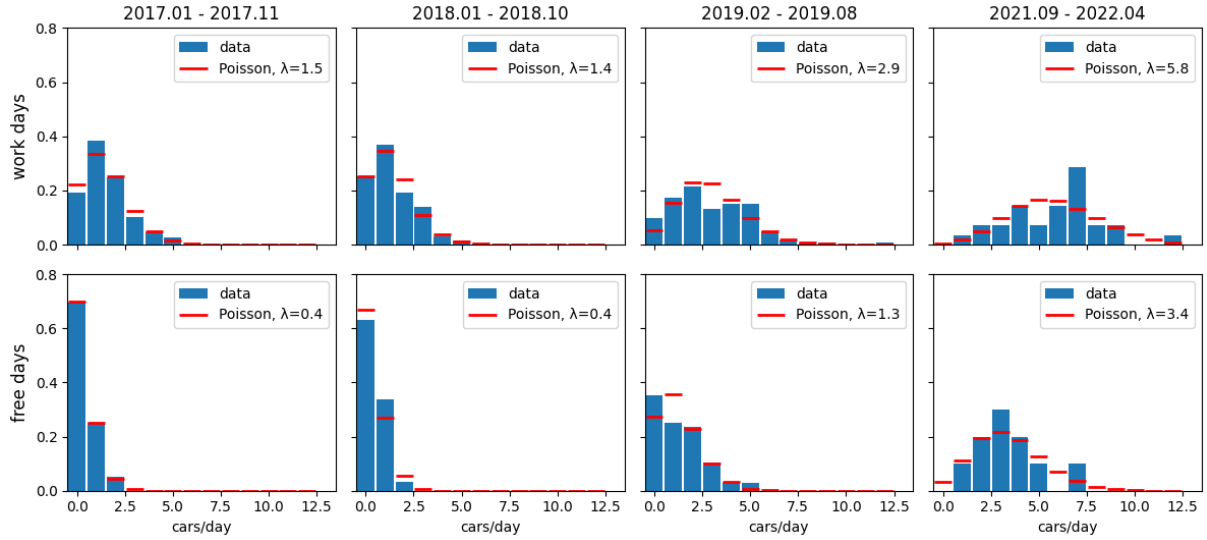


Figure 2.13: Probability distributions for the amount of cars refueling per day. Several periods with relatively stationary behaviour (refer to Fig. 2.11) are analysed separately. The blue bars show the empirical distribution, while the red lines show the results from the Poisson distribution. Based on visual inspection of the figure, the Poisson distribution is sufficiently accurate.

2.5.2 Time of refuelling events

Next, a distribution is created for the the arrival time of cars. The distribution is significantly different for for work days and for free days, so two distributions are created with a bin size of one hour. It is not fitted to a distribution function because no functions fit the data shape well. Instead, the discrete distribution is used directly in subsequent models.

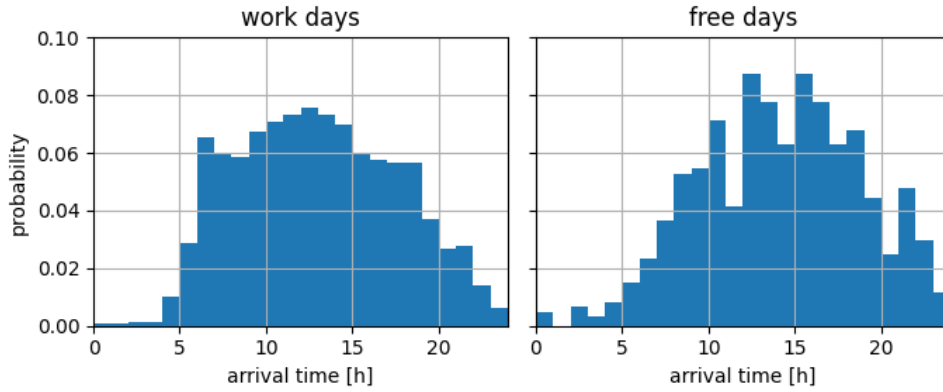


Figure 2.14: Empirical probability distribution P_T for the arrival time of cars. The bin size is 1 hour. A uniform distribution is assumed within each bin.

2.5.3 Amount refuelled

Lastly, a distribution for the amount of hydrogen refuelled per car needs to be found. This distribution is not significantly different between work days and free days, so one distribution for all days is used.

2.5.4 Statistical model

In several historical years, the hydrogen demand shows an increasing or decreasing trend due to an increase or decrease in active customers. These trends do not represent typical seasonal behaviour, so we don't want to include them in the analysis. Therefore, the real data is replaced by artificial, stationary timeseries of the hydrogen demand. These artificial timeseries could also be used to create scenarios for

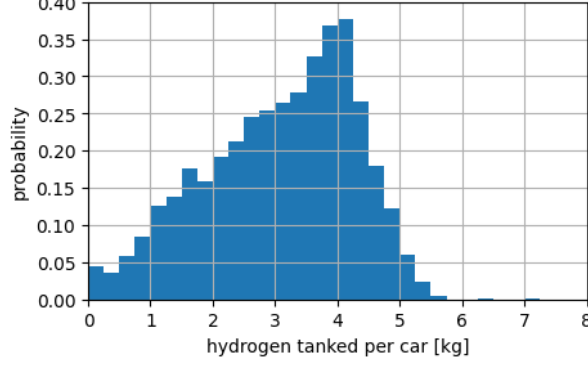


Figure 2.15: Empirical probability distribution P_M for amount of hydrogen refueled by a car. The bin size is 0.25 kg. A uniform distribution is assumed within each bin.

stochastic MPC. They are created as follows:

Algorithm 1: Create synthetic hydrogen demand timeseries

```

1 set the average arrival rate  $\lambda_a$ ;
2 for every day do
3   determine the day type (work/free) and its specific arrival rate  $\lambda$  using ratio  $\frac{\lambda_w}{\lambda_a}$  or  $\frac{\lambda_f}{\lambda_a}$ ;
4   sample the number of cars from the Poisson distribution  $P_N$  according to Eq. 2.13;
5   for every car do
6     sample time from distribution  $P_T$  according to Fig. 2.14;
7     sample hydrogen amount from distribution  $P_M$  according to Fig. 2.15;
8   end
9 end
10 gather all cars in a dataframe and resample to the desired time resolution;
```

For SDDP optimization, we need a discrete probability distribution for the amount of hydrogen refuelled in each hour. First, the average car arrival rate for a specific hour is determined using

$$\lambda_h = P_T(h) \cdot \lambda_d \quad (2.14)$$

where λ_d is the average arrival rate for that day, $P_T(h)$ is the probability of a refuelling event happening during hour h of the day and λ_h is the resulting average arrival rate for that hour. The distribution for the amount of hydrogen refuelled within that hour is then given by the discrete compound Poisson distribution $B = M_1 + \dots + M_N$ where B indicates the total amount of hydrogen tanked in an hour and M_n indicates the hydrogen mass tanked by the n th car arriving that hour. This distribution is given by

$$P_B(b) = \sum_{n=0}^{\infty} P_N(n) \cdot P_M^{*n}(b) \quad (2.15)$$

where P_M^{*n} is the n th convolution of P_M with itself:

$$P_M^{*n}(b) = \sum_{k=-\infty}^{\infty} P_M^{*(n-1)}(k) \cdot P_M(b-k) \quad (2.16)$$

Since P_M is separated into bins of 0.25 kg, the distribution P_B is also separated into bins of 0.25 kg. This is too precise and makes SDDP slow. Therefore, bins are merged into 1 kg steps, using the weighted average of the merged bins as the new mass value. The highest bins with low probability are further merged into one bin. Table 2.3 shows the refuelled-mass-per-hour distribution for a specific hour.

Table 2.3: Discrete probability distribution for amount of hydrogen tanked on a workday from 12:00-13:00.

mass [kg]	0.00	0.58	1.53	2.53	3.54	4.39	5.35	6.50	7.49	8.44	9.39	11.49
probability	0.7911	0.0104	0.0279	0.0424	0.0588	0.0466	0.0084	0.0048	0.0045	0.0030	0.0011	0.0009

2.6 PV production and predictions

Data of PV production was extracted directly from the EHUB Platform.

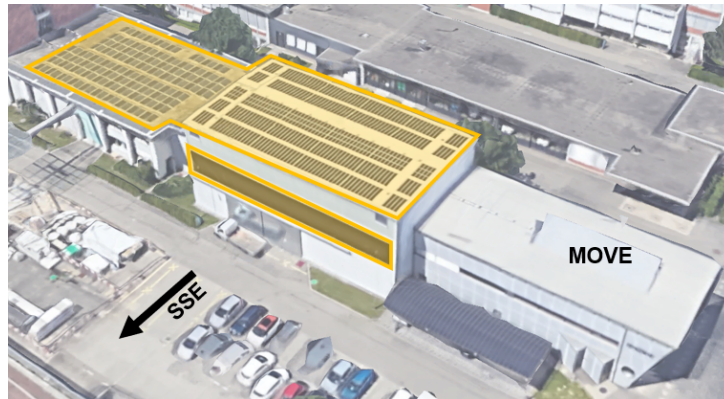


Figure 2.16: Photovoltaic panels included in the MOVE-system. There is 549 m² of roof PV and 84 m² of façade PV, resulting in a total capacity of 73 kWp.

2.7 Day-ahead electricity prices

The day-ahead electricity prices from 2015 onwards were obtained from the ENTSO-E Transparency Platform [14].

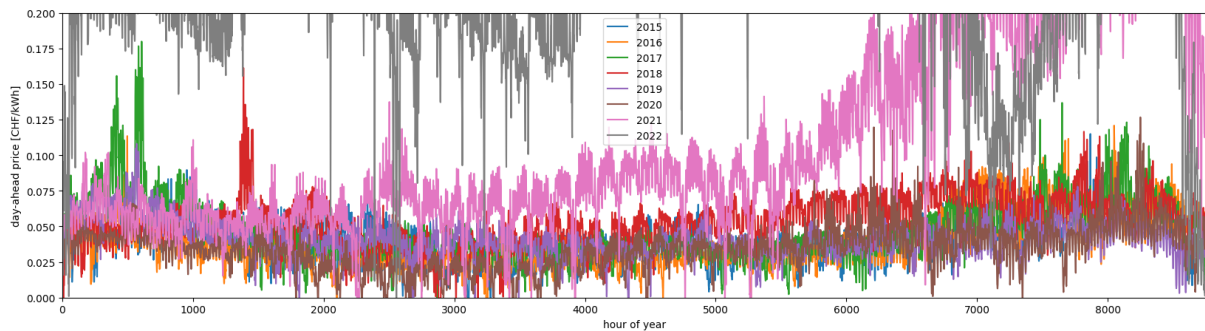


Figure 2.17: Day-ahead prices from the ENTSO-E Transparency Platform [14]. Prices after April 2021 are not used since those prices are atypical.

Chapter 3

Control Algorithm

This chapter demonstrates a control algorithm for the flexible operation of the MOVE system shown in Fig. 2.1. The objective is to operate the system for minimum cost under day-ahead electricity prices. This means that the control algorithm optimizes *Flexibility for Energy*. *Flexibility for Power* is addressed in Chapter 4. The flexible control algorithm has a special focus on exploiting flexibility at timescales longer than a week. These timescales can have major added value in Power-to-Hydrogen systems, but are usually not addressed in Model Predictive Control (MPC) due to limitations in computational tractability. The proposed control algorithm mitigates these limitations by combining different models and algorithms. Fig. 3.1 shows the components of the control algorithm. The proposed algorithm is tested on the year 2019.

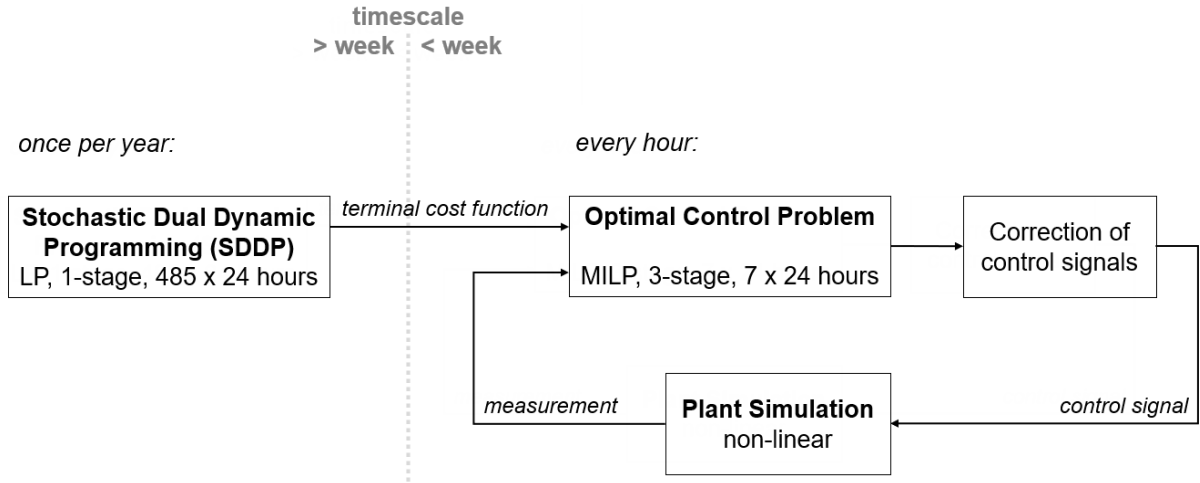


Figure 3.1: Flowchart of the proposed flexible control algorithm. The SDDP algorithm addresses timescales longer than a week. It performs an offline optimization of the single-stage, linear model over a time horizon of 485 days with hourly resolution and produces a set of terminal cost functions. Timescales shorter than a week are addressed by online MPC. The Optimal Control Problem (OCP) is a MILP optimization problem that optimizes the three-stage mixed-integer linear model of MOVE over a horizon of 7 days with hourly resolution. After optimization, the control signals are corrected and applied to the plant, which is the non-linear simulation model in this thesis. Measurements from the simulation are used as the initial states of the OCP in the next timestep.

3.1 Terminal cost function

As introduced in Section 1.3, MPC is a technique for the control of flexible energy systems. It decides what control inputs to apply to the system based on the optimal solution of the Optimal Control Problem (OCP), which contains a model of the system, a cost function and predictions of future disturbances. This optimization is repeated regularly, with initial states updated from measurements. Unfortunately, MPC often fails to take into account the long term. The hydrogen tanks in MOVE hold enough hydrogen

to refuel vehicles for an average of 11 days, which implies that the storage can provide flexibility in the timescale of weeks. Moreover, we are interested in a possible connection to an energy hub with buildings, where the hydrogen storage would assume a seasonal balancing function. These time horizons cannot be properly addressed by conventional MPC. As a solution, a terminal cost term is often included in the objective function of the OCP, resulting in the general form

$$\begin{aligned}
u_t = \arg \min_{u_t} \quad & \sum_{t=1}^T C(u_t) \quad + V_{T+1}(x_{T+1}) \\
\text{s.t.} \quad & x_{t+1} = T(x_t, u_t, d_t) \quad \forall t \in \{1, \dots, T\} \\
& u_t \in U, x_t \in X, x_{T+1} \in X \quad \forall t \in \{1, \dots, T\} \\
& x_1, U, X, d_t \text{ given}
\end{aligned} \tag{3.1}$$

where t is the timestep index. $T(x_t, u_t, d_t)$ is a transition function that maps state variables x_t , control inputs u_t and disturbances d_t to the state variable in the next timestep x_{t+1} . $C(u_t)$ is the cost associated with the control inputs. U is the set of feasible control inputs while X is the set of feasible state variables. $V_{T+1}(x_{T+1})$ is the terminal cost function. The terminal cost is the minimum cost to complete the remaining problem, beyond MPC horizon T . The terminal cost *function* $V_{T+1}(x_{T+1})$ is the terminal cost as a *function* of state variable x_{T+1} , which is the state of x at the end of MPC horizon T .

In MOVE, the state variable is the mass of stored hydrogen. The more hydrogen in the storage, the cheaper it will be to complete the remaining problem, because you can empty the storage. Without terminal cost function, the storage would always be empty at the end of the optimized horizon. The terminal cost function represents the value that the stored hydrogen has in the remainder of the problem. As such, it takes into account the remainder of the problem beyond the optimized horizon. With the terminal cost function, the hydrogen storage won't typically be empty at the end of the optimized horizon because it has value.

However, determining the terminal cost function is non-trivial. In a previous case study on MOVE [23], a constant marginal value is attributed to the stored hydrogen, based on the estimated cost of hydrogen production, derived from average efficiencies, PV production and electricity prices during a certain time period. This heuristic method is non-generalizable and has no proof. In fact, logical analysis of MOVE reveals two hypotheses that undermine the use of a constant value.

Hypothesis 1: In summer, there is more PV production and the electricity prices are generally lower than in winter. This suggests that the value of hydrogen in storage is not constant, but varies over the year, with a lower value in spring/summer.

Hypothesis 2: Stored hydrogen is first used to replace production during the most expensive moments (highest electricity prices and lowest PV production). After that, ever less expensive moments follow. So, the first "bit" of hydrogen is used for the most expensive moments. This suggests that the marginal value of stored hydrogen is highest when the tank is almost empty, and lowest when the tank is almost full.

Darivianakis et al.[9] does a better attempt at obtaining a value function for a P2H2P system. An optimization of the system with a five year time horizon is solved for more than 100 historical and synthetic scenarios. It is found that the hydrogen tank purely functions as seasonal storage, therefore the state of charge follows a similar path in all scenarios. This allows to only calculate the value function $V_t(x_t)$ at the two bounds of this path ($\underline{x}_t, \bar{x}_t$) for each timestep and to interpolate between them. The value function is calculated by optimizing the rest of the year over all scenarios with x_t as initial state. However, this method cannot be applied to MOVE since its hydrogen storage provides flexibility in the timescale of days to weeks, not just seasonal flexibility. As a result, the state of charge path is not similar in all scenarios. Next to that, performing long-horizon optimizations for two initial states at every time step might become computationally restrictive.

3.2 Dual Dynamic Programming

As shortly discussed in Section 1.3, the Stochastic Dual Dynamic Programming (SDDP) algorithm [32], introduced in 1991, is typically used for scheduling of multiple interconnected hydropower reservoirs, over long time horizons, under stochastic conditions. This thesis researches whether the method is transferable

to the scheduling of Power-to-Hydrogen(-to-Power) systems, as it has the exact same needs. For simplicity, we start with the deterministic version of the SDDP algorithm, Dual Dynamic Programming (DDP).

In MPC, the entire problem (with all its timesteps) is solved at once. DDP uses the principle of Dynamic Programming and Bellman's equation[3], splitting the problem into *subproblems*. Each subproblem consists of the cost function and transition function of one timestep plus the terminal cost function of the next timestep. Only one subproblem, i.e. only one timestep, is solved at once. The terminal cost function of a timestep equals the optimal solution of that timestep's subproblem:

$$\begin{aligned} V_t(x_t) = \min_{u_t, x_{t+1}} \quad & C_t(u_t) + V_{t+1}(x_{t+1}) \\ \text{s.t.} \quad & x_{t+1} = T(x_t, u_t, d_t) \end{aligned} \quad (3.2)$$

So, the terminal cost functions link the timesteps together. This allows to iterate forwards and backwards through the timesteps of the problem, always solving just one subproblem at a time. DDP builds a *lower approximation of the terminal cost function* while iterating forwards and backwards through the timesteps. The update of the terminal cost function bases on the principle of duality: in a LP, the dual variables can be interpreted as the marginal cost associated with a change of the state variables. This allows to add a hyperplane to the approximate terminal cost function. DDP is typically used for linear problems but can be extended to the nonlinear case. Optimal solutions are only guaranteed for convex problems. Fig. 3.2 explains the DDP algorithm in more detail.

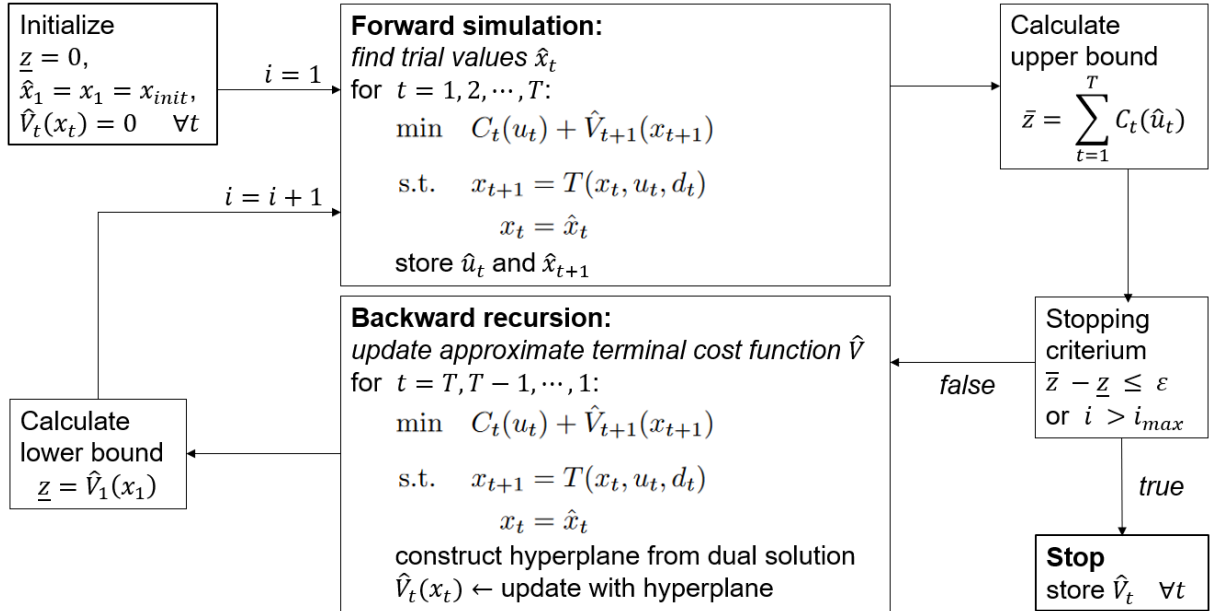


Figure 3.2: Flowchart of the Dual Dynamic Programming (DDP) algorithm, slightly simplified for the sake of understandability. First, all approximate terminal cost functions $\hat{V}_t(x_t)$ are initialized as zero. Then, the forward simulation iterates forward through the timesteps and finds the optimal trial values \hat{u}_t and \hat{x}_{t+1} . Then, the backwards recursion iterates through the timesteps in reverse. Each subproblem is solved and the dual solution is used to add a hyperplane to the terminal cost function. This terminal cost function is then used in the previous subproblem, etc. The algorithm is stopped when the total cost of the forward simulation (upper bound) and the terminal cost function of the first timestep (lower bound) are sufficiently close together.

It turns out that in any convex LP, the exact terminal cost function is piecewise linear and convex [32][15]. This proves hypothesis 2 for all cases without negative electricity prices. Since the convexity is in the direction of minimization, the piecewise linear value function can be used in the OCP without introducing extra binary variables or nonlinearities.

SDDP has been used as control algorithm on its own, but it could also be used to feed terminal cost functions back to the Optimal Control Problem. Flamm et al.[15] use a combination of MPC and DDP for the optimization of a a electrolyzer/fuel cell system for seasonal storage under day-ahead electricity prices. The OCP is nonlinear with a horizon of 3 days and 1-hour sample period. The DDP is a linear

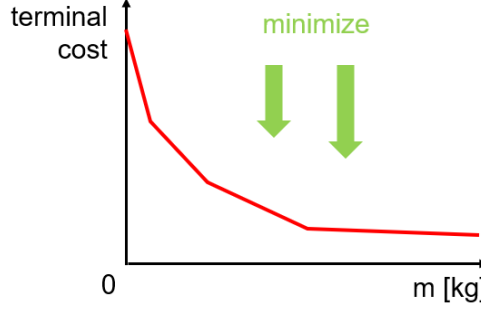


Figure 3.3: Piecewise-linear, convex terminal cost function.

relaxation of the problem. The two are coupled with the terminal cost function at the timestep where the two algorithms meet. They report near-optimal solutions over horizons of multiple months.

This thesis explores an approach which builds on the one used by Flamm et al. [15]. First, the DDP problem is solved offline for one year. The time horizon is chosen from January 1st of the analysed year until May 1st of the next year, under the assumption that seasonal storage devices have completed their cycles by then [9]. Also, May 1st is far enough into the next year to not influence flexible behaviour in the timescale of weeks in the analysed year. It produces approximate, convex, piecewise linear terminal cost functions for each hour of the year. These terminal costs functions are then used online, every hour, in the Optimal Control Problem of the MPC.

3.2.1 Application to MOVE

The DDP algorithm is implemented in the open-source package SDDP.jl [12] in the Julia programming language. SDDP.jl is built on JuMP.jl, a Julia package that provides a modeling language for optimization problems. JuMP supports multiple open-source and commercial solvers. In this thesis, DDP optimization problems are solved using SDDP.jl with the open-source HiGHS solver. Due to the effort of the SDDP.jl contributors, the double work of implementing SDDP is avoided.

For DDP, the MOVE system is modelled as an LP. All three hydrogen storages are grouped into one storage for the sake of simplicity, resulting in a single-stage model. The 440 bar compressor turns on immediately when the electrolyser produces hydrogen, and the 900 bar compressor is turned on immediately when a car refuels. This simplification means that the total compressor power is accurate, but the time at which compression happens is shifted and not flexible as in the real world. Since DDP is suitable for handling multiple interconnected reservoirs, the problem could be extended to a three-stage problem rather easily in future work. The single-stage LP model results in the following subproblem for each timestep:

$$\hat{V}_t(m_t) = \min \quad \left(C_t^{dayahead} \cdot (P_t^{grid,imp} - P_t^{grid,exp}) + C^{fix} \cdot P_t^{grid,imp} + C^{nofill} \cdot \dot{m}_t^{nofill} \right) \cdot \Delta t + \hat{V}_{t+1}(m_{t+1}) \quad (3.3a)$$

$$\text{s.t.} \quad P_t^{el} = \eta^{el} \cdot \dot{m}_t^{el} \quad (3.3b)$$

$$P_t^{comp440} = \eta^{comp440} \cdot \dot{m}_t^{el} \quad (3.3c)$$

$$P_t^{comp900} = \eta^{comp900} \cdot \dot{m}_t^{exp} \quad (3.3d)$$

$$P_t^{PV} + P_t^{grid,imp} - P_t^{el} - P_t^{comp440} - P_t^{comp900} - P_t^{grid,exp} = 0 \quad (3.3e)$$

$$m_{t+1} = m_t + (\dot{m}_t^{el} - \dot{m}_t^{exp} + \dot{m}_t^{nofill} - \dot{m}_t^{vent}) \cdot \Delta t \quad (3.3f)$$

$$m_{t+1}^{min} \leq m_{t+1} \leq m_{t+1}^{max} \quad (3.3g)$$

$$0 \leq \dot{m}_t^{el} \leq \dot{m}_t^{el,max} \quad (3.3h)$$

$$P_t^{grid,imp}, P_t^{grid,exp}, \dot{m}_t^{nofill}, \dot{m}_t^{vent} \geq 0 \quad (3.3i)$$

$$C_t^{dayahead}, C^{fix}, C^{nofill}, \dot{m}_t^{el,max}, \dot{m}_t^{exp}, m_{t+1}^{min}, m_{t+1}^{max} \text{ given.} \quad (3.3j)$$

where the subscript t denotes the t -th time step. Δt denotes the timestep size, P denotes electrical power, m denotes hydrogen mass in the (aggregated) storage, \dot{m} denotes hydrogen mass flow rate, C

denotes cost and η denotes efficiency in kWh kg^{-1} . Superscripts denote the associated device, with *PV* for photovoltaic panesl, *el* for electrolyser, *comp440* for the 440 bar compressor, *comp900* for the 900 bar compressor, *exp* for hydrogen refuelling (export) and *grid* for electricity grid. The only control variable is \dot{m}_t^{el} , i.e. the electrolyser mass flow. The subproblem consists of the following equations:

- 3.3a** Objective function. The day-ahead electricity price $C_t^{dayahead}$ is associated with the balance of grid imports $P_t^{grid,imp}$ and grid exports $P_t^{grid,exp}$. C^{fix} represents the fixed grid cost associated only with electricity imports. This fixed grid costs consists of network tariffs and taxes. It is set to 0.1284 CHF/kWh, which is the median for Switzerland in 2023 for the C2 user category[36]. The value could easily be adjusted to exactly represent 2019, but this is not critical as fixed grid costs are similar between years. C^{nofill} and \dot{m}_t^{nofill} are explained in constraint 3.3f. The last component of the objective function is the terminal cost function of the next timestep $\hat{V}_{t+1}(m_{t+1})$, which is a function of the mass at the beginning of the next timestep.
- 3.3b** Mass flow to power relationship of the electrolyser. Since it is not possible to include a binary variable due to the linear requirement, an average electrolyser efficiency of 60% is used, which corresponds to $65.67 \text{ kWh kg}^{-1}$.
- 3.3c** Mass flow to power relationship of the 440 bar compressor. Due to the simplification to a single-stage model, it is assumed that this compressor compresses any hydrogen produced by the electrolyser immediately, so that compressor mass flow equals electrolyser mass flow \dot{m}_t^{el} .
- 3.3d** Mass flow to power relationship of the 900 bar compressor. Due to the simplification to a single-stage model, it is assumed that any hydrogen exported for refuelling is compressed by the 900 bar compressor in the same timestep. So, the compressor mass flow equals the hydrogen demand \dot{m}_t^{exp} .
- 3.3e** This constraint states that the power balance must be zero. No binary variable is needed to ensure mutual exclusivity between $P_t^{grid,imp}$ and $P_t^{grid,exp}$ since the presence of fixed cost C^{fix} only related to electricity imports already ensures mutual exclusivity in the optimal solution.
- 3.3f** Update of the hydrogen mass in the storage tank. Hydrogen produced by the electrolyser is added while hydrogen refuelled is subtracted. Furthermore, there are the auxiliary variables \dot{m}_t^{nofill} and \dot{m}_t^{vent} . These are needed since DDP requires all subproblems to be feasible at all times. \dot{m}_t^{nofill} is an artificial hydrogen source to prevent infeasibility when the stored mass is lower than the refuelled mass in a subproblem. Due to the high associated cost C^{nofill} in the objective function, \dot{m}_t^{nofill} will amount to zero in the optimal solution. C^{nofill} can be interpreted as a penalty for load not served, i.e. cars not able to completely fill their tanks. \dot{m}_t^{vent} represents hydrogen vented out of the storage tank and prevents infeasibility when the storage mass constraints tighten due to rising temperature. \dot{m}_t^{vent} will also amount to zero in the optimal as wasting hydrogen is not optimal.
- 3.3g** The storage mass constraints. These are different for each timestep due to different tank temperature at each timestep.
- 3.3h** Constraint for minimum and maximum mass flow of the electrolyser.

The optimization problem is solved for 2019. Historical PV data is used as described in Chapter 2. As hydrogen demand, synthetic data from the statistical model described in Chapter 2 is used since the real hydrogen demand is non-uniform over 2019, which complicates the study of seasonal effects. An average arrival rate of 2.6 cars per day is used. The storage limits (m_t^{min}, m_t^{max}) depend on the storage tank temperatures, for which the average of the four temperature measurements is taken. This temperature is converted to mass constraints using the Lemmon equation (2.2, 2.3). Day-ahead electricity prices are retrieved from the ENTSO-E Transparency Platform.

3.2.2 Results

The DDP problem was solved on a laptop with Intel®Core™i7 processor and 16 GB RAM. After 80 iterations of training the problem, which takes 22 minutes, the gap between upper and lower bound is 257 CHF. After 130 iterations, which takes 42 minutes, the gap between upper and lower bound is 0.4 CHF. In 2019, 3240 kg of hydrogen is refuelled for a total production cost of CHF 27165, resulting in an average hydrogen cost of 8.38 CHF/kg. The simulated results are shown in Fig. 3.4 for the full time horizon and in Fig 3.5 for a selected week in May-June. The hydrogen storage shows 6 (nearly) full discharges in 2019. This suggests that the storage acts on the timescale from weeks to months, providing flexibility for weather spells and periods of high or low prices. The storage gets charged when electricity prices are low or when high electricity prices are foreseen in the future. In the weekly plot (Fig. 3.5), it can be seen that the MOVE system also provides flexibility on the daily and hourly timescale. It always follows the PV power during the day and turns off at night. When electricity prices

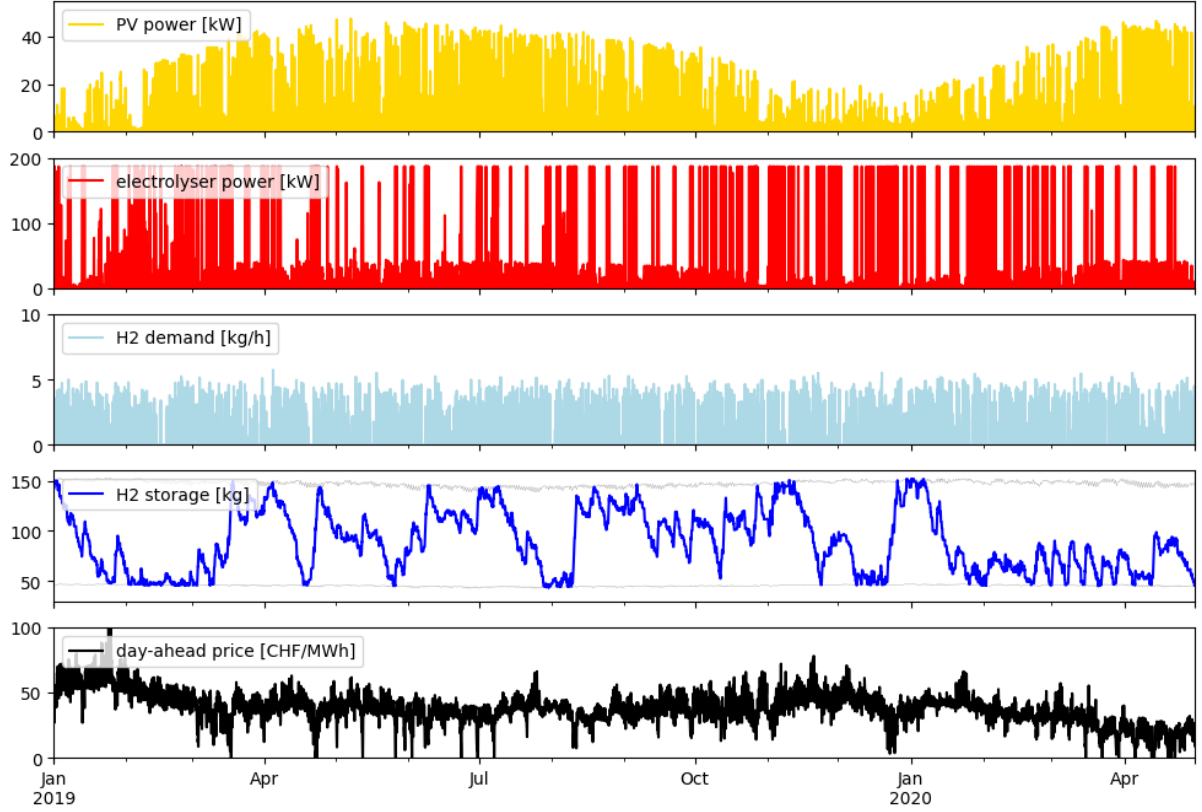


Figure 3.4: DDP results: simulation of optimal policy over 16 months.

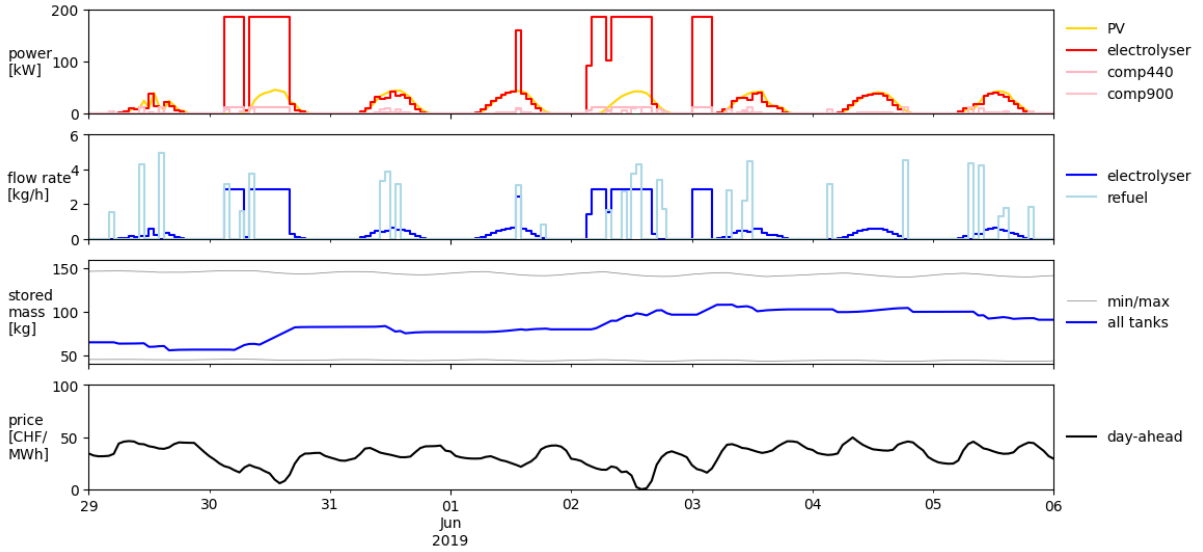


Figure 3.5: DDP results: simulation of optimal policy over 16 months, zoomed in on a week in May/June. There are 6 full discharges of the storage in 2019.

are low, the electrolyser is turned to full power, independent of PV availability.

The resulting marginal values of stored hydrogen are shown in Fig. 3.6. These marginal values visualize the terminal cost functions. The results confirm hypothesis 1 and 2: At higher fill levels, the marginal value is lower than at low fill levels. At low fill levels, the marginal value is strongly affected by the penalty for hydrogen load not served (C^{nofill}). The marginal value of stored hydrogen is higher in autumn and winter and lower in summer and spring, which relates to the availability of solar energy and the price levels. A detailed analysis of the marginal values is performed in section 3.3.1.

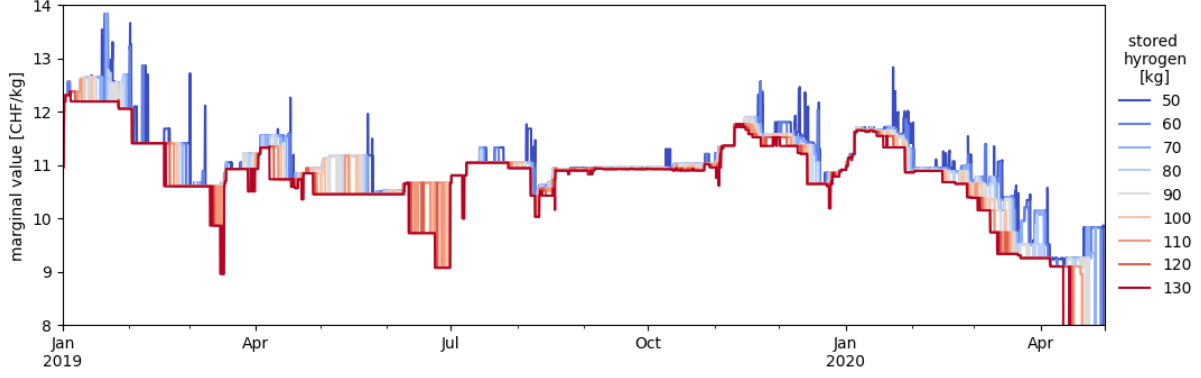


Figure 3.6: DDP results: marginal value of stored hydrogen. The marginal value indicates the decrease in terminal cost when the fill level is increased by 1 kg, departing from the fill level indicated by the color. The drop in marginal value around Jan 2020 is due to lower energy prices during the winter holidays. The marginal values after 1 Jan 2020 should not be used since they are too close to the end of the horizon.

3.3 Stochastic Dual Dynamic Programming

DDP can be extended to the stochastic case, Stochastic Dual Dynamic Programming (SDDP) [32]. SDDP is also implemented in SDDP.jl [11]. SDDP works in a similar way to DDP (Fig. 3.2), but uses *expected* cost and *expected* terminal cost functions. In the forward simulation, a Monte Carlo sample of the random variables is used to find trial values \hat{x} . In the backward recursion, each subproblem is solved for each possible realization of stochasticity. The approximate terminal cost function is then updated using the probability of each possible realization as weight. This way of handling stochasticity in the backward recursion *requires a complete stochastic model* for each stochastic variable and this stochasticity should be *discretized*. The more discrete realizations of stochasticity, the more subproblems need to be solved. So, the solve time grows linearly with the amount of discrete realizations of stochasticity. Although SDDP has several advantages such as recursivity, no need to discretize states and no curse of dimensionality, the requirement of discrete stochastic variables is a disadvantage. A detailed explanation of SDDP is found in [32] and [11]. The Bellman's equation belonging to SDDP is as follows:

$$\begin{aligned} \mathbb{E}[V_{t,s}(x_t)] &= \min_{u_t, x_{t+1}} C(u_t, \mathbf{c}_{t,s}) + \mathbb{E}_{s \in S_{t+1}} [V_{t+1,s}(x_{t+1,s})] \\ \text{s.t.} \quad x_{t+1} &= T(x_t, u_t, \mathbf{d}_{t,s}) \\ \mathbf{d}_{t,s} &\in D_{t,s}, \quad \mathbf{c}_{t,s} \in C_{t,s} \\ u_t &\in U, \quad x_t, x_{t+1} \in X \end{aligned} \quad (3.4)$$

where the subscript s represents the Markov state (explained later in this section). The bold variables are stochastic variables, with $\mathbf{c}_{t,s}$ for stochastic electricity prices and $\mathbf{d}_{t,s}$ for stochastic disturbances, i.e. PV power and hydrogen demand.

Fig. 3.7 shows how the stochasticity of MOVE was integrated in the SDDP model. The hydrogen demand is stagewise-independent and a statistical model for it was already presented in section 2.5.4. This probability distribution is summarized in Table 2.3. Therefore, it is easy to integrate into SDDP. The discrete probability distribution for hydrogen demand is applied separately to every timestep. There is a different probability for work days and free days and for each hour of the day.

The solar PV production and electricity prices are harder to integrate, since they are stagewise-dependent, which SDDP cannot handle in its pure form. A common approach to handle stagewise-dependence in SDDP is to model the system as a Markov chain. Especially solar irradiation can be modeled very well as Markov chain. Markov chains can be represented by policy graphs (Fig. 3.7). Markov chains are nodes with transition probabilities between the nodes. The amount of solar irradiation hitting the outside of the atmosphere is deterministic and dependent on the hour of day and day of the year. Cloud cover causes the solar irradiation on ground to be stochastic. Cloud cover can be separated into three types: Clear, partially cloudy and cloudy. During clear days, it is easy to predict irradiation while during cloudy days it is hard because it is much more variable. The clear, partially cloudy and cloudy weather can each be modeled as its own row (Markov state) in the Markovian policy graph, allowing for different stochastic

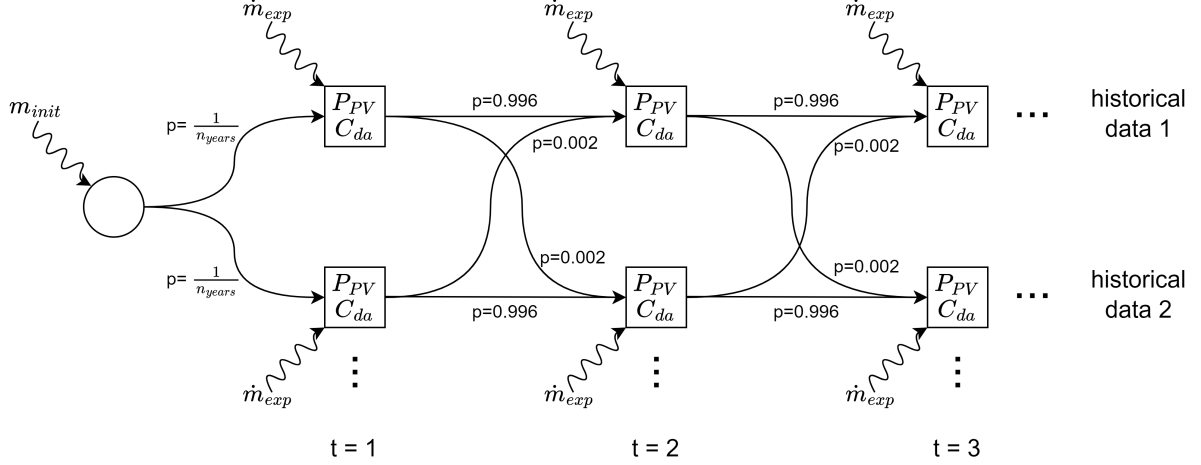


Figure 3.7: Markovian policy graph of the SDDP model of MOVE. Each square represents one timestep t and one Markov state s . The columns represent timesteps. The rows represent the different Markov states, in this case the different years of historical data. Each row of historical data consists of day-ahead electricity prices C_{da} and PV power P_{pv} . The wiggly lines represent the discrete probability distribution for hydrogen demand that is applied separately to each timestep since it is stagewise-independent. The straight and curved arrows represent the probability of transitioning between nodes. The transition probability is chosen such that on average, there is a switch between Markov states every 10 days. The circle represents the root node. There is an equal probability of switching from the root node to each row of historical data, so that all historical years are equally represented. A random initial mass is applied to the root node so that all storage fill levels are explored in the beginning of the year.

realizations for different nodes at the same timestep. The probability of staying in the same Markov state is higher than the probability of changing. Solar models based on Markov chains are detailed in [5],[1],[40] and [25]. Additionally, an auto-regressive process can be included in SDDP by making stochastic variables dependent on a previous state. This process, suitable for electricity spot market prices, is described in [10].

Establishing these statistical models for solar irradiation and electricity prices is a difficult task which is outside the scope of this thesis. However, an approximation can be made using scenario trees [34]. This thesis explores a simplified method using scenario trees. The historical data of solar irradiation (2020-2023) and electricity prices (2015-2018) during three years are taken. Every year is represented by one row in the Markovian policy graph. So, instead of sampling from statistical models, we sample from historical data. Since we are only using three years, we are likely overfitting to these three years of historical data. Also, it would be better to use the same year for both electricity prices and PV power in each historical data row. However, this is the best data we have at the moment. To keep stagewise-dependence but not simply end up with optimizations for 3 years, there is a certain probability of transitioning between the different historical data rows. The probability of staying in the same historical data row is 0.996, so that on average, a scenario switch is made every 10 days. These 10 days were chosen heuristically, as it seems sufficiently long to capture stagewise-dependence in weather but short enough for sufficient switching between scenarios. Also, it is desirable to not have a fixed initial value. This is achieved by starting the first node at the minimum fill level and adding a stochastic amount of "free" hydrogen in the first timestep.

The solve time is 8 hours for 230 iterations on a laptop with 16 GB RAM and i7 Processor. The long duration is not necessarily a problem since the optimization would be performed offline, once per year or whenever the long-term predictions change considerably. The solve time can be shortened by exploiting parallel processing and using a commercial solver such as GUROBI.

3.3.1 Results

Unfortunately, directly simulating 2019 is not possible with the Markovian version of SDDP. Instead, a simulation is done on a sampled path through the three different years, as would be done during the forward simulation. The results are shown in Fig. 3.8. The graph shows that the system is still relatively

well able to fill the storage during cheaper periods, although it makes less full charging cycles than in the deterministic simulation.

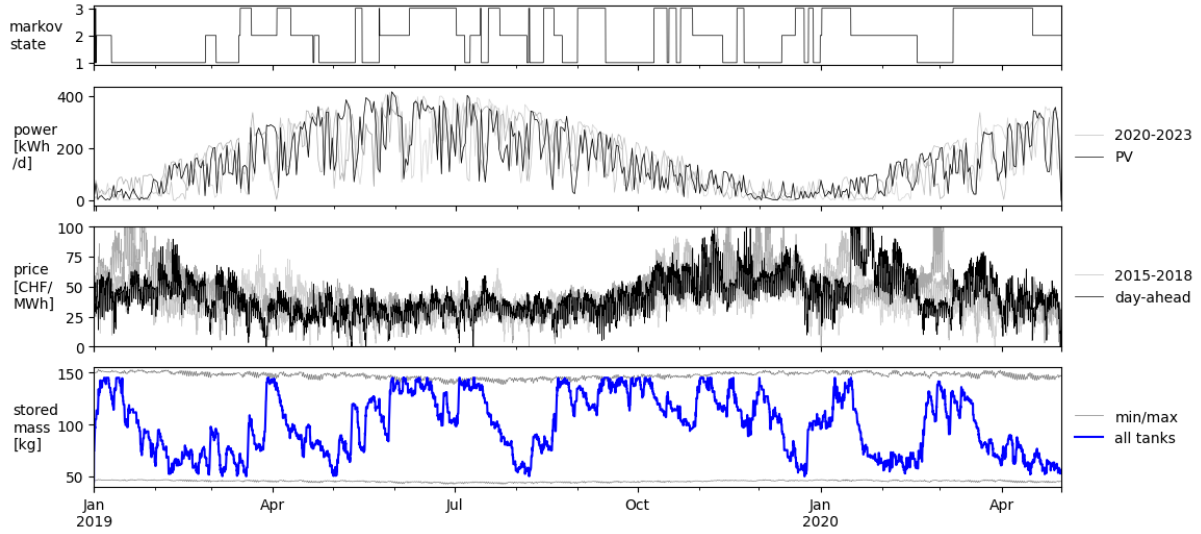


Figure 3.8: SDDP results: simulation of optimal policy over 16 months. Black lines show the simulated path while the grey lines show the realizations of the other historical years that have been used to find the optimal policy. The bottom plot shows the storage level of the aggregated hydrogen tank. The top plot shows the markov state, i.e. the year that is sampled at a certain timestep.

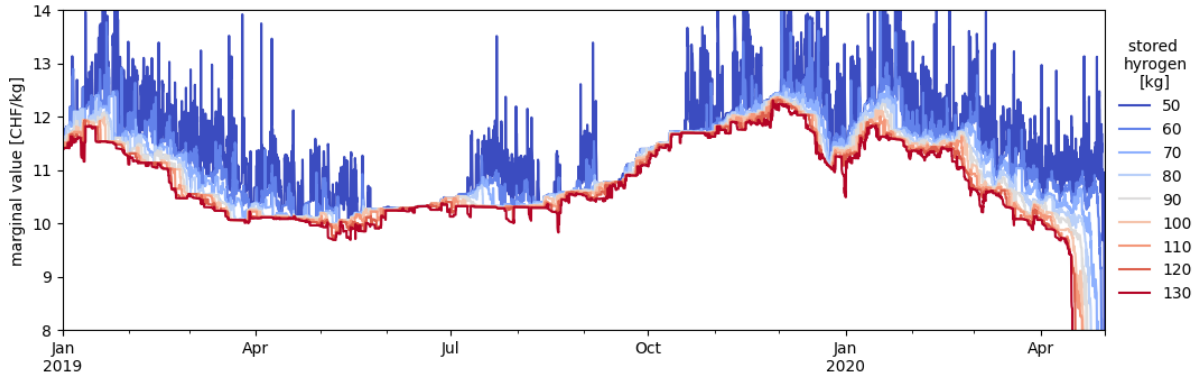


Figure 3.9: SDDP results: marginal value of stored hydrogen. The marginal value indicates the decrease in terminal cost when the fill level is increased by 1 kg, departing from the fill level indicated by the color. The drop in marginal value around Jan 2020 is due to lower energy prices during the winter holidays. Around July and October, the low storage levels show no spikes in marginal value. This is because low storage states were explored in none of the scenarios during this period.

SDDP creates a approximate terminal cost function for each timestep, for each markov state. The final terminal cost functions that are used in the Optimal Control Problem, are obtained with the following process:

1. Sample terminal cost and marginal price at several fixed mass levels of the storage.
2. Take the unweighted average over the three Markov states (since there is equal probability of being in each year) for each timestep.
3. To create terminal cost function for OCP: create piecewise-linear function from the sampled and averaged terminal costs for each timestep.

The result is a series of marginal values attached to each timestep and each mass level of the storage as well as the terminal cost function for each timestep. Fig. 3.9 shows the marginal hydrogen values resulting from SDDP. The spread of marginal values is higher than in the deterministic scenario since more storage states were explored due to stochasticity.

The average cost of hydrogen in the sampled simulation is 8.52 CHF/kg, while the marginal value of

stored hydrogen is between 10 and 12 CHF/kg. This is because the marginal cost of hydrogen is not equal to the average cost of hydrogen. The MOVE system has a limited amount of PV power available. The more hydrogen it needs to produce, the more it needs to use the more expensive grid electricity. As a result, the marginal cost of hydrogen increases as the hydrogen demand increases. For example, if the marginal value of the storage is 12 CHF/kg, you would always put hydrogen into the storage if you can produce it for less than 12 CHF/kg. However, the marginal value cannot be interpreted as the selling price of hydrogen since the model does not assume one fixed hydrogen price. It *can* be interpreted as the extra cost when 1 more kg of hydrogen would be refuelled, on top of the predicted demand. In future research, it would be interesting to adapt the model to determine the price of hydrogen.

3.4 Model Predictive Control

In this section, the MILP Optimal Control Problem is formulated that is used for MPC. The reason for using MILP is that it allows to model the difference between off and standby mode for the electrolyser, as well as the electrolyser startup period, but it is more tractable than non-linear optimization. The OCP optimizes towards minimum cost under day-ahead electricity prices and is repeatedly solved at every timestep. First, some notation is introduced. The subscript t denotes the t -th time step in the prediction horizon. Δt_t denotes the timestep size, P denotes electrical power, m denotes hydrogen mass, \dot{m} denotes hydrogen mass flow rate, C denotes cost and $f_x(\cdot)$ denotes a piecewise linear function. Superscripts denote the associated device, with *el* for electrolyser, *comp* for compressor, *st* for storage tank and *grid* for electricity grid. The three storage tanks are modeled individually, with the superscripts *low*, *mid* and *high* referring to the 30, 440 and 900 bar tanks respectively. The control variables are the set $U = \{u_t^{mode}, \dot{m}_t^{el}, \dot{m}_t^{comp440}, \dot{m}_t^{comp900}\}$. They represent the on/off mode and mass flow rate of the electrolyser and the mass flow rates of both compressors. All quantities without subscript t are given parameters. The problem is formulated under the assumption of strictly positive day-ahead electricity prices $C_t^{dayahead}$, which avoids binary variables and allows to model equality constraints as inequality constraints.

$$\min_{U, S} \sum_{t=1}^T \left[\left(C_t^{dayahead} \cdot (P_t^{grid,imp} - P_t^{grid,exp}) + C_{grid,fix} \cdot P_t^{grid,imp} + C^{nofill} \cdot \dot{m}_t^{nofill} \right) \cdot \Delta t_t \right] + C^{term} \quad (3.5a)$$

$$\text{s.t. } u_t^{el,mode} \in \{0, 1\} \quad \forall t \in \{1, \dots, T\} \quad (3.5b)$$

$$\dot{m}_t^{el} \leq \dot{m}^{el,max} \cdot u_t^{el,mode} \quad \forall t \in \{1, \dots, T\} \quad (3.5c)$$

$$\dot{m}_t^{el} \leq f_{el,mtx} \left(m_t^{st,low}, T_t^{st} \right) \text{***not implemented in final version} \quad \forall t \in \{1, \dots, T\} \quad (3.5d)$$

$$P_t^{el,on} \geq f_{el}(\dot{m}_t^{el}) \quad \forall t \in \{1, \dots, T\} \quad (3.5e)$$

$$P_t^{el} \geq P_t^{el,on} + M \cdot (1 - u_t^{mode}) \quad \forall t \in \{1, \dots, T\} \quad (3.5f)$$

$$P_t^{el} \geq P^{el,off} \quad \forall t \in \{1, \dots, T\} \quad (3.5g)$$

$$P_{t-1}^{el,start} \geq \frac{E^{el,start}}{\Delta t_{t-1}} \cdot (u_t^{el,mode} - u_{t-1}^{el,mode}) \quad \forall t \in \{2, \dots, T\} \quad (3.5h)$$

$$u_0^{el,mode} \leq u^{el,mode,prev} \quad (3.5i)$$

$$P_t^{comp440} = \eta^{comp440} \cdot \dot{m}_t^{comp440} \quad \forall t \in \{1, \dots, T\} \quad (3.5j)$$

$$P_t^{comp900} = \eta^{comp900} \cdot \dot{m}_t^{comp900} \quad \forall t \in \{1, \dots, T\} \quad (3.5k)$$

$$P_t^{comp440} \leq P^{comp440,max} \quad \forall t \in \{1, \dots, T\} \quad (3.5l)$$

$$P_t^{comp900} \leq P^{comp900,max} \quad \forall t \in \{1, \dots, T\} \quad (3.5m)$$

$$P_t^{PV} + P_t^{grid,imp} - P_t^{el} - P_t^{el,start} - P_t^{comp440} - P_t^{comp900} - P_t^{grid,exp} = 0 \quad \forall t \in \{1, \dots, T\} \quad (3.5n)$$

$$\dot{m}_t^{el} - \dot{m}_t^{comp440} + \dot{m}_t^{st,low} = 0 \quad \forall t \in \{1, \dots, T\} \quad (3.5o)$$

$$\dot{m}_t^{comp440} - \dot{m}_t^{comp900} + \dot{m}_t^{st,mid} = 0 \quad \forall t \in \{1, \dots, T\} \quad (3.5p)$$

$$\dot{m}_t^{comp900} - \dot{m}_t^{exp} + \dot{m}_t^{st,high} + \dot{m}_t^{nofill} - \dot{m}_t^{vent} = 0 \quad \forall t \in \{1, \dots, T\} \quad (3.5q)$$

$$m_{t+1}^{st,p} = m_t^{st,p} + \dot{m}_t^{st,p} \cdot \Delta t \quad \forall p \in \{low, mid, high\} \quad \forall t \in \{1, \dots, T\} \quad (3.5r)$$

$$m_t^{st,p,min} \leq m_t^{st,p} \leq m_t^{st,p,max} \quad \forall p \in \{low, mid, high\} \quad \forall t \in \{1, \dots, T+1\} \quad (3.5s)$$

$$C^{term} \geq f_T^{term} \left(m_{T+1}^{st,low} + m_{T+1}^{st,mid} + m_{T+1}^{st,high} \right) \quad (3.5t)$$

$$P_t^{el,on}, P_t^{el}, P_t^{el,start}, P_t^{comp440}, P_t^{comp900}, P_t^{grid,imp}, P_t^{grid,exp} \geq 0 \quad \forall t \in \{1, \dots, T\} \quad (3.5u)$$

$$\dot{m}_t^{el}, \dot{m}_t^{comp440}, \dot{m}_t^{comp900}, \dot{m}_t^{nofill}, \dot{m}_t^{vent} \geq 0 \quad \forall t \in \{1, \dots, T\} \quad (3.5v)$$

With decision variables

$$S = \{P_t^{el,on}, P_t^{el}, P_t^{el,start}, P_t^{comp440}, P_t^{comp900}, P_t^{grid,imp}, P_t^{grid,exp}, \\ \dot{m}_t^{el}, \dot{m}_t^{comp440}, \dot{m}_t^{comp900}, \dot{m}_t^{nofill}, \dot{m}_t^{vent}, \\ \dot{m}_t^{st,low}, \dot{m}_t^{st,mid}, \dot{m}_t^{st,high}, \\ m_t^{st,low}, m_t^{st,mid}, m_t^{st,high}, \\ C^{term}\},$$

given parameters

$$D = \{u^{el,mode,prev}, m_1^{low}, m_1^{mid}, m_1^{high}, \\ \dot{m}^{el,max}, P^{comp440,max}, P^{comp900,max}, \eta^{comp440}, \eta^{comp900}, E^{el,start}, \\ m_t^{st,p,min}, m_t^{st,p,max}, T_t^{st}, \Delta t_t, \\ C_t^{dayahead}, C^{grid,fix}\},$$

and the following constraints:

- 3.5b-c** constrains the electrolyser mass flow \dot{m}_t^{el} to the maximum flow rate $\dot{m}^{el,max}$ when the electrolyser is turned on and to zero when the electrolyser is turned off. u_t^{mode} is the only binary variable in the problem and is the on/off control variable for the electrolyser.
- 3.5d** implements the mass flow limit due to the pressure gradient between the electrolyser and buffer (2.6). The function $f_{el,mtx}(m_t^{st,low}, T_t^{st})$ is a concave piece-wise linear function. As the function defines an upper limit, it can be implemented as separate linear constraints. The limit is a function of the hydrogen mass in the 30 bar tanks $m_t^{st,low}$ and the temperature of the storage tanks T_t^{st} , which is given as deterministic parameter. In the final version, this constraint was not implemented as it is very specific to the MOVE system and increases solve time.
- 3.5e** represents the piecewise linear relationship between mass flow and electrolyser power $P_t^{el,on}$ in the on mode. In fact, this should be an equality constraint but since electrolyser power is minimized in the objective function, it can be modeled as an inequality constraint. $f_{el}(\dot{m}_t^{el})$ is a piecewise linear, convex function. Since it defines a lower limit, it can be modeled as separate linear constraints, avoiding the use of binary variables. However, modeling the inequality constraint as an equality constraint is only valid when electricity prices are strictly positive. Yet, negative day ahead prices happen for about 100 hours per year. Therefore, the electricity price data is pre-processed to have a minimum price of 1 CHF/MWh. It is assumed that this does not greatly affect the results, as the electrolyser will still tend towards full production at these hours due to the low electricity price. In the analysis of the results, the original electricity prices can be used.
- 3.5f-g** uses the binary variable u_t^{mode} and a big M constraint to distinguish between the electrolyser power P_t^{el} in the on and off mode. In the off mode, the electrolyser power equals the given constant $P^{el,off}$. In the on and standby mode, $P_t^{el} = P_t^{el,on}$. Again, equality constraints are modeled as inequality constraints under the assumption of positive electricity prices.
- 3.5h-i** model the electrolyser power during cold start-up $P_t^{el,start}$. The constant startup energy $E^{el,start}$ is assigned as an average power in the previous timestep when the current timestep is a startup. This is calculated by $u_t^{mode} - u_{t-1}^{mode}$. In the last timestep, the startup power is zero. Constraint 3.5j prevents a start-up in the first time step. This is explained later.
- 3.5j-m** define the maximum capacity and the mass flow-power relationships of the compressors.
- 3.5n** is the energy balance for electrical power. $P_t^{grid,imp}$ and $P_t^{grid,exp}$ represent the power imported from and exported to the grid, respectively. Both are non-negative and add up to the total grid power $P_t^{grid,imp} - P_t^{grid,exp} = P_t^{grid}$. These should be mutually exclusive, which would require an extra binary variable. However, the fixed grid cost $C^{grid,fix}$ (=0.1284 CHF/kWh as in the DDP problem) associated only with imported grid power ensures that $P_t^{grid,imp}$ is always minimized, automatically enforcing mutual exclusivity. This is proven by the fact that when both are nonzero, it is always possible to reduce $P_t^{grid,exp}$, which in turn reduces $P_t^{grid,imp}$.
- 3.5o-q** implement the energy balances for the three hydrogen pressure levels. $\dot{m}_t^{st,low}$, $\dot{m}_t^{st,mid}$ and $\dot{m}_t^{st,high}$ indicate the mass flow into the 30, 440 and 900 bar tanks, respectively. \dot{m}_t^{exp} represents the hydrogen demand, given as average mass flow during the timestep. \dot{m}_t^{nofill} is a virtual hydrogen

source that prevents infeasibility in scenarios with (multiple) refuelling events in the first timesteps of the time horizon. A cost of 200 is associated with \dot{m}_t^{nofill} in the objective function, so that the model is motivated to avoid infeasibility. This 200 can be interpreted as the penalty for customers not being able to refuel their car. \dot{m}_t^{vent} is a slack variable, which allows the model to vent hydrogen when the upper constraint tightens due to a temperature rise.

3.5r is the update of the storage tanks.

3.5s are the storage tank limits. These limits are given parameters based on the expected tank temperature.

3.5t associates a terminal cost C_{term} with the hydrogen mass in the tanks at the last timestep. When there is more hydrogen in the tanks, the terminal cost will be lower. The terminal cost is calculated with the value function $f_T^{term} \left(m_{T+1}^{st,low} + m_{T+1}^{st,mid} + m_{T+1}^{st,high} \right)$ which is obtained from the results of the SDDP optimization. The masses of all tanks are grouped together, since the SDDP uses only a single storage. Since the marginal value of hydrogen is thus the same in all tanks and there is a cost associated to the use of compressors, the model is motivated to keep the hydrogen as much as possible at low pressure levels at the end of the time horizon. This creates a sub-optimality. Since the time horizon is sufficiently long and the compressor can only operate flexibly over a time frame of a few hours, it is assumed that this does not affect model results prohibitively. However, since SDDP is built to handle interconnected storages in hydropower systems, it is expected that separate value functions for the three storages can be generated with a small change to the model.

3.5u-v implement non-negativity constraints for several variables.

The timestep size of the problem is one hour, (except for the first timestep, see section 3.4.1). Using a variable timestep size, for example splitting up the first few hours into 15 minutes, could be a way to increase accuracy without affecting computational speed too much. This was also done in [20], where short timesteps are used in the short-term horizon and long timesteps in the long-term horizon. However, in this thesis only hour-based PV predictions are available and also the electricity prices are constant during every hour. Therefore, just the hourly timestep is chosen.

Contrary to Laaksonlaita [23], it was found that solve time is not significantly reduced when grouping the storage tanks into one variable. Therefore, the three-stage model is kept because it is more accurate without big penalties. Instead, binary variables and interdependencies between state variables and immediate variables, such as the mass transport limit (Eq. 3.5d), slow down the problem.

The problem is considered as optimal when the absolute tolerance gap between the optimal LP equivalent and the MILP is below 0.1 CHF/day. More optimal solutions are possible below this tolerance but the improve in objective function is not significant in real life. The increase of the tolerance significantly improves solve time.

3.4.1 Correction of control signals

Post-optimization correction of the control signals plays an important role in reducing the complexity of the optimization problem.

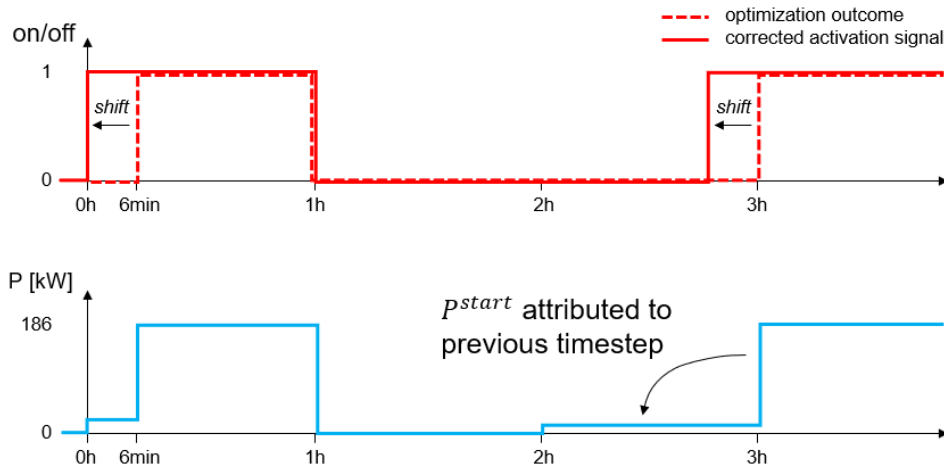


Figure 3.10: Correction of the activation signal before it is applied to the plant.

Firstly, control signal correction allows for modelling the cold start-up of the electrolyser (Fig. 3.10). The first hour is split into two timesteps for the purpose of modelling the electrolyser start-up period. The MPC is optimized every hour. In the optimization problem, the electrolyser produces at full power immediately when u_t^{mode} switches to 1 and the startup power is assigned to the previous timestep. However, in real life the electrolyser has to switch on 6 minutes beforehand, which is the startup duration. Therefore, the u_t^{mode} signal at the start of each operation period is shifted forward by 6 minutes in the correction. The u_t^{mode} of the first hour are then used to run the system. In the next hour, the optimization is repeated, etc. The first timestep is 6 minutes so that the algorithm is accurate also when the MPC decides to turn on the electrolyser, even though this was not planned in the previous optimization. The modelling of the startup period does cause a slight increase in solve time, so for long time horizons it should be omitted.

Secondly, the setpoint u_t^{sp} for the mass flow controller is derived from the intended electrolyser mass flow rate \dot{m}_t^{el} after optimization. This allows for a nonlinear relationship between setpoint and mass flow.

Thirdly, the optimization results are evaluated to check whether the implicit constraints are really met. This is not absolutely needed but gives peace of mind.

Fourth, post-processing of the optimization results has the potential to allow negative electricity prices without having to introduce binary variables for the electrolyser efficiency $f_{el}(\dot{m}_t^{el})$. To do this, the curve would be upper bounded with a linear equation. Then, in post processing the actual electrolyser power is calculated based on the mass flow rate. Any surplus power that was present in the optimization result can be used to waste energy in a cheap device such as a resistance heater or turning on lights. Further details on how to adapt the problem for negative energy prices are in the appendix.

3.4.2 Deterministic MPC with perfect foresight

The deterministic MPC with perfect foresight of the future was run for a prediction horizon of 7 days with an hourly resolution. 7 days is a period in which weather and future electricity prices can be predicted with a meaningful probability and the solve time is still reasonable. The problem is solved in 2-50 seconds depending on the initial storage states and the parameters over the prediction horizon. The DDP terminal cost functions are used. Fig. 3.11 shows the results.

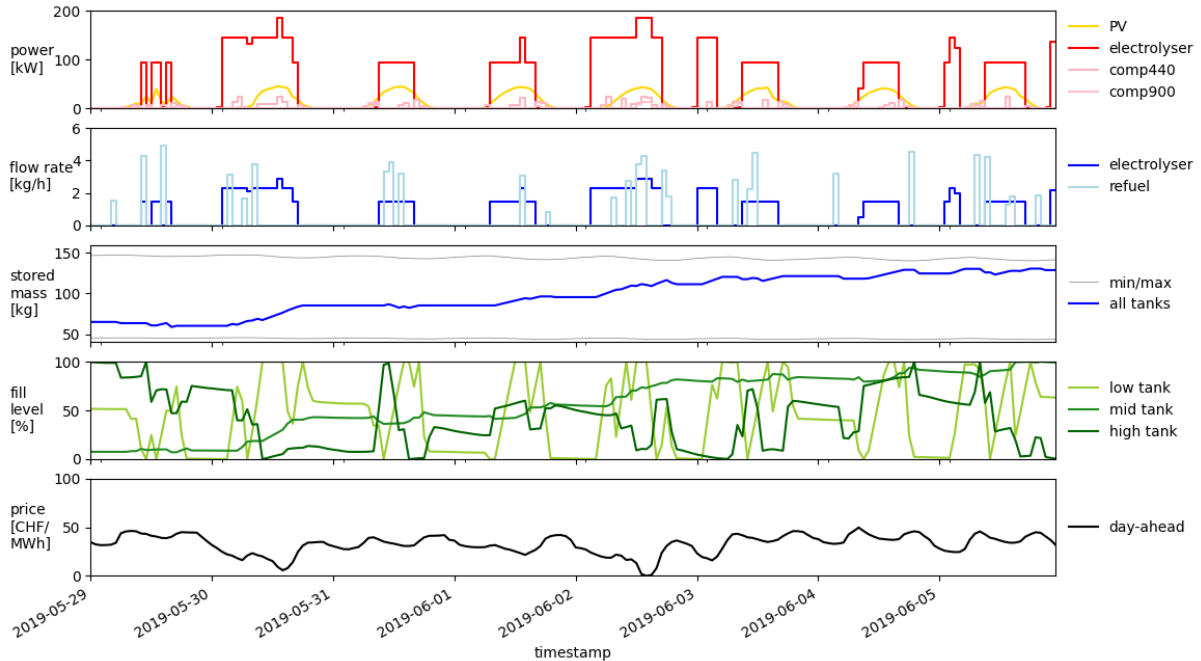


Figure 3.11: Optimization results for a week in May/June

If the terminal cost function from DDP was completely correct, the path followed by SDDP and MPC would be exactly the same. This is not the case, suggesting that the terminal cost function is not completely accurate. It is very probable that this is caused by the discrepancy that the MPC is a MILP and the SDDP is an LP. A clear difference between the MPC (Fig. 3.11) and SDDP results 3.5 is the

operation of the electrolyser. In the LP, the electrolyser follows the PV power, operating at low load, which is not penalized due to the fixed efficiency number. The MILP has a much better equation for the efficiency of the electrolyser depending on the part load. Since the electrolyser is inefficient at low loads, the electrolyser in the MILP doesn't follow the PV directly but rather lets the electrolyser only operate from a minimum load level. This difference in LP and MILP behaviour can be the cause of the inaccuracy in terminal cost function. Although different, the optimal storage path of the MPC is still quite similar to the SDDP path. This suggest that the terminal cost function is at least in the right range.

3.4.3 Deterministic MPC with imperfect foresight

To perform deterministic MPC with imperfect foresight, the same optimization problem (Eq. 3.5) is used. However, instead of deterministic inputs the inputs as shown in Fig. 3.12 are used. This is done to evaluate the performance of the MPC in case of non-perfect predictions. The focus in this thesis was not on creating prediction models, so average profiles of the historical data were used for the parts of the MPC horizon where no informed prediction is available.

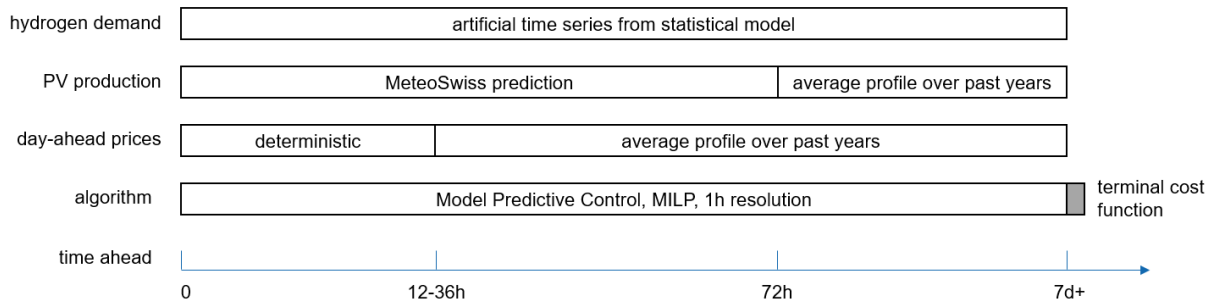


Figure 3.12: Overview of inputs to the Optimal Control Problem in case of imperfect foresight.

Chapter 4

Flexibility Assessment

In this chapter, the flexibility of MOVE is assessed. In the first section, the flexibility envelope of the MOVE system is found and reported.

4.1 Flexibility Envelope

The concept of the flexibility envelope was already introduced in section 1.1.5. The flexibility envelope concept is from [16] and [7]. The goal of the flexibility envelope is to communicate to a DSO or virtual power plant how much flexibility a system can offer. It does so by communicating the maximum duration that a certain power level can be sustained. The system should be able to deliver this power level at a signal of the DSO. This means that the feasibility of these power level should be guaranteed. As such, it is important to take into account the worst case scenario when calculating the guaranteed available duration. This is especially relevant because the hydrogen demand is stage-wise independent. This means that no good prediction can be made about the future hydrogen demand, other than information from the statistical model. The considered horizon is maximum 24 hours. The PV power is removed from this analysis since it is considered a non-controllable load in this thesis and the flexibility envelope of curtailable PV is described in [7].

4.1.1 Maximizing power

When maximizing power, the optimization objective is to consume as much power as early as possible. Because we need high probability that we can actually deliver this power level, we need to assume a worst case scenario. As such, the problem can be interpreted as a robust optimization problem. In case of power maximization, the worst case is when the energy demand is very low. This corresponds to zero cars coming to refuel during 24 hours. Based on an average of 2.6 cars refuelling per days, the probability of zero cars refuelling is 4.5% during work days and 22.5% during free days. This is sufficient probability to take zero hydrogen demand during 24 hours as a worst case scenario. The resulting optimization problem is:

$$\begin{aligned}
\min \quad & \sum_{t=1}^{25} \left(-e^{-\frac{t}{5}} \cdot P_t^{grid} + 1000 \cdot \dot{m}_t^{vent} + 1000 \cdot \dot{m}_t^{nofill} \right) \cdot \Delta t_t \quad (4.1a) \\
\text{s.t.} \quad & \text{all constraints from the MPC problem 3.5, except 3.5d, 3.5n and 3.5t} \quad (4.1b) \\
& P_t^{grid} - P_t^{el} - P_t^{comp450} - P_t^{comp900} = 0 \quad \forall t \in \{1, \dots, T\} \quad (4.1c) \\
& P_t^{el,on} \leq 60.1 \cdot \dot{m}_t^{el} + 16 \quad \forall t \in \{1, \dots, T\} \quad (4.1d) \\
& P_t^{el} \leq P_t^{el,on} \quad \forall t \in \{1, \dots, T\} \quad (4.1e) \\
& P_t^{el} \leq P_t^{el,off} + M \cdot u_t^{mode} \quad \forall t \in \{1, \dots, T\} \quad (4.1f) \\
& P_{t-1}^{el,start} \leq \frac{P_t^{el,start} \cdot t_t^{el,start}}{\Delta t} \cdot u_t^{mode} \quad \forall t \in \{1, \dots, T\} \quad (4.1g) \\
& P_{t-1}^{el,start} \leq \frac{P_t^{el,start} \cdot t_t^{el,start}}{\Delta t} \cdot (1 - u_t^{mode}) \quad \forall t \in \{1, \dots, T\} \quad (4.1h) \\
& P_t^{grid} \geq 0 \quad \forall t \in \{1, \dots, T\} \quad (4.1i)
\end{aligned}$$

4.1c represents the new power balance. P_t^{PV} and $P_t^{grid,exp}$ are taken out of the problem. P_t^{grid} represents the power from the grid and is the variable that we want to maximize to happen as early as possible. This goal is achieved by applying the cost function $-e^{-\frac{t}{5}}$, which means that the cost for the same power level is much lower at earlier timesteps. 4.1d-h are needed because we are now rewarding power consumption in the objective function, so that we cannot rely on inequality constraints to act as equality constraints anymore. Note that the electrolyser power in the on mode is now approximated as a linear function. For more detailed analysis, this can be changed to the piecewise linear function from 3.5. \dot{m}_t^{vent} and \dot{m}_t^{nofill} are slack variables to prevent infeasibility but are heavily penalized so that they amount to zero after optimization unless feasibility was encountered. The coefficients 5, 1000 and 1000 in the objective function 4.1a are carefully chosen relative to each other so that the cost of using slack variables is always higher than the cost associated with grid electricity.

This optimization problem is repeated for every timestep. The power levels and their maximum durations are extracted from the cumulative sum of energy consumption at each $t \in \{1, \dots, T\}$. The first timestep, which has $\Delta t = 6$ minutes, is skipped in this analysis. Therefore, the resulting flexibility envelope represents the amount of power that can be made available within 6 minutes. In this simple problem it would also be relatively easy to obtain an analytical solution for the maximum flexibility envelope.

4.1.2 Minimizing power

When minimizing power, the optimization objective is to consume power as late and little as possible. Again, we need high probability that this power level can actually be delivered. In this case, the worst case scenario is when many cars refuel a large amount of hydrogen as early as possible.

However, it is hard to determine what is a reasonable worst case, since a small chance of infeasibility should be allowed to prevent being too conservative. There is a 10% chance that more than 18 kg of hydrogen gets refuelled during a work day. Using this information, a worst case scenario is established heuristically, with hydrogen demand of 6, 4, 0, 5, 0 and 3 kg of hydrogen in the first 5 hours and zero for all other hours. Additionally, these refuelling events are assumed to happen at the beginning of each hour, so that the usable mass in the 900 bar tank has to at least the amount that will be refuelled in the next timestep. Additionally, the compressor is required to always fill back to full 900 bar tank as soon as possible. It leads to the following optimization problem:

$$\begin{aligned}
\min \quad & \sum_{t=1}^{25} \left(e^{\frac{25-t}{10}} \cdot P_t^{grid} + 1000 \cdot \dot{m}_t^{vent} + 2500 \cdot \dot{m}_t^{nofill} \right) \cdot \Delta t_t + 100 \cdot \left(m_t^{st,high,max} - m_t^{st,high} \right) \quad (4.2a) \\
\text{s.t.} \quad & \text{all constraints from the MPC problem 3.5, except 3.5n and 3.5t} \quad (4.2b) \\
& P_t^{grid} - P_t^{el} - P_t^{comp450} - P_t^{comp900} = 0 \quad \forall t \in \{1, \dots, T\} \quad (4.2c) \\
& m_t^{st,high} \geq m_t^{st,high,min} + \dot{m}_t^{exp} \quad \forall t \in \{1, \dots, T\} \quad (4.2d) \\
& P_t^{grid} \geq 0 \quad \forall t \in \{1, \dots, T\} \quad (4.2e)
\end{aligned}$$

where 4.2c again represents the new power balance. 4.2d implements the constraint that enough hydrogen should be available to refuel the cars in the next timestep. In the objective function, a cost of 100/kg is attributed to the 900 bar tank not being full. Again, \dot{m}_t^{vent} and \dot{m}_t^{nofill} are heavily penalized slack variables to prevent infeasibility in case the 900 bar tank fill level is too low to fill the first cars or when the capacity constraints change due to changing temperatures. Again, the coefficients 25, 10, 1000, 2500 and 100 in the objective function 4.1a are carefully chosen relative to each other so that the cost of using slack variables is always higher than the cost associated with grid electricity. Specifically, the cost of \dot{m}_t^{nofill} was increased to 2500 to be more expensive than the cost of a non-full 900 bar tank. In the future, a non-heuristic way of determining suitable coefficients should be found.

4.1.3 Combined flexibility envelope

The combined flexibility envelope is obtained by taking

$$duration = \min \left(duration_t^{powmin}(P), \quad duration_t^{powmax}(P) \right) \quad (4.3)$$

for every power level P , for every timestep t . Durations < 0 are considered as power levels that cannot be guaranteed.

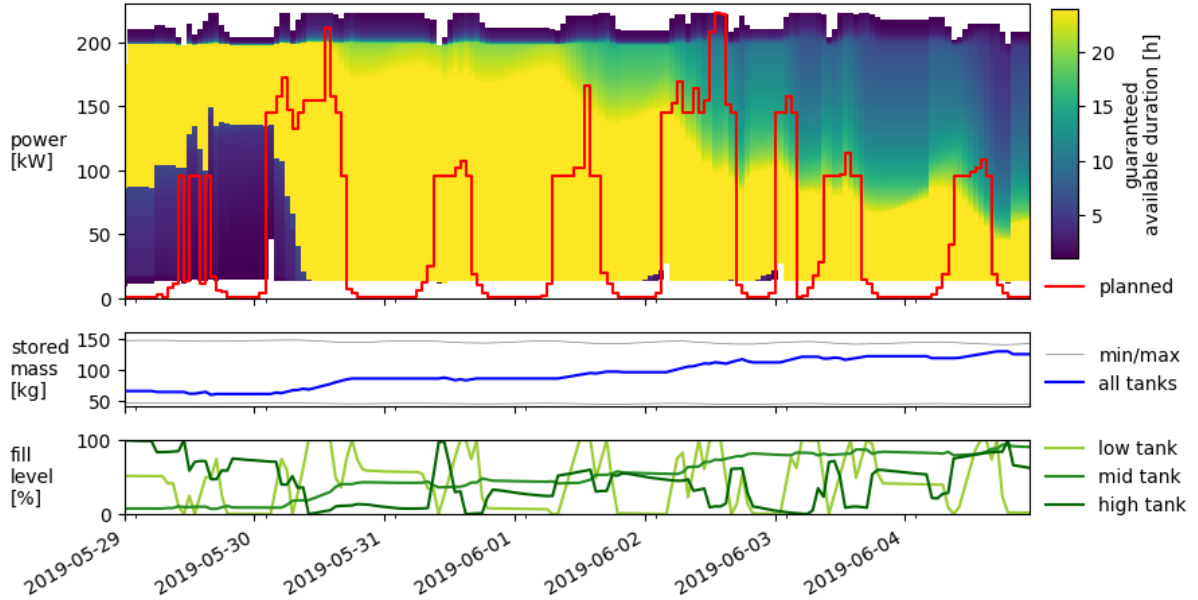


Figure 4.1: Flexibility envelope for a week in May-June. The colors represent the maximum duration for which a power level can be guaranteed, when initialized with the state variables in the corresponding timestep. The white areas indicate power levels are either (a) infeasible or (b) might be feasible, but cannot be guaranteed. The standard power level is the planned power level that will happen when no flexibility requests occur.

Several things can be observed from the flexibility envelope:

- As the tanks reach a higher fill level, maximum power can be sustained for a shorter time.

- The varying upper power bound is due to the compressors and the spread of mass between the tanks. If the target tank is full, the compressor cannot make its power available. Furthermore, the compressors are constrained by the mass flow rate of the electrolyser and the mass in the source tank.
- The 12 kW band of non-available power at the minimum levels is due to the rule introduced for the compressor, which says that the 900 bar tanks should always be filled up immediately. A car could arrive at any time, and so it is not possible to guarantee a power level below 12 kW.
- Unlike the upper bound, the lower power bound has very sharp drops in guaranteed duration when going from one power level to the next. This is due to the non-convex energy bounds.
- In some cases, the planned power level overlaps with non-guaranteed power levels. This is possible since the day-ahead optimization does not consider worst-case scenarios.

Generally, it can be concluded that the electrolyser and compressors offer a large amount of flexibility. Most flexibility is offered by the electrolyser. When the stored hydrogen mass is somewhere in the middle of the usable range of the tanks, the system can offer nearly its entire power range for more than 24 hours. When the storage tanks come closer to the upper bound, higher power levels are possible for shorter duration. When the fill levels of the storage tanks are low, the behaviour is more unpredictable. If many cars happen to refuel very early, and the 440 bar tanks are also close to their lower bounds, the electrolyser might be forced to turn on, requiring a high power level. However, when there is at least 18 kg of hydrogen in the tanks, the problem is soon resolved as the chance that more than 18 kg is refuelled during one day is rather low.

This envelope shows the flexibility of the electrolyser when it is already in the on mode. Before real use, another envelope graph should be created to communicate the reaction time with the DSO. The resultant flexibility envelope can be communicated to an aggregator or DSO, who can require the MOVE system to provide a certain power level at their signal. The originally planned power levels should also be communicated with the DSO.

An interesting follow up study would be to obtain the initial states from an optimization that does not only optimize on the day-ahead market, but already takes into account the possibility of flexibility offering, as was done in [16]. To achieve this, research on a remuneration scheme for offering flexibility using the flexibility envelope is needed.

Chapter 5

Conclusion and Discussion

5.1 Conclusion

Power-to-Hydrogen(-to-Power) systems are highly flexible at timescales from second to seasonal due to their fast dynamics and low cost per unit of stored energy. Flexible operation increases the profitability of these systems. However, flexible control methods often fail to take into account timescales longer than a week.

The first contribution of this thesis is the identification of a control-oriented model of the MOVE system, utilizing a MILP model. This model extends previous work [23] by incorporating the cold-start period of the electrolyser, which is crucial for assessing system flexibility. Additionally, a statistical model based on the compound Poisson distribution is introduced to model stochastic hydrogen demand. The result is a discrete probability distribution for the hydrogen mass refuelled in each hour.

The second contribution is the proposed flexible control method that takes into account timescales from one hour to seasonal. Several models and algorithms are combined to achieve this goal. The Stochastic Dual Dynamic Programming (SDDP) algorithm performs an offline optimization of a linearized model of MOVE over a horizon of 16 months. SDDP yields convex, piecewise-linear terminal cost functions for each hour of the year. The terminal cost functions quantify the value of stored hydrogen. They show that the value of stored hydrogen is not constant, but varies during the year and depending on the fill level of the tank. The convex, piecewise-linear terminal cost functions are used in the mixed-integer linear Optimal Control Problem of a real-time Model Predictive Control (MPC) algorithm. The resulting control signals are corrected before application to the system plant: the electrolyser activation signal is shifted forward to take the startup period into account. To the best of our knowledge, the combination of offline SDDP and online MPC has not been shown before.

The third contribution is the application of the flexibility envelope to the MOVE system, which allows to communicate the *Flexibility for Power* potential with a system operator. To obtain the flexibility envelope, the MILP optimization problem was reformulated with a different objective function. Worst-case scenarios were used to find the power levels and durations that could be guaranteed. The analysis reveals that the MOVE system exhibits high flexibility when the hydrogen storage is not near its upper or lower pressure bounds.

In conclusion, the thesis demonstrates the effectiveness of the SDDP algorithm in assessing the value of stored energy at seasonal timescales and generating terminal cost functions for each hour of the year. These terminal cost functions can be incorporated into other control problems to account for time beyond the prediction horizon. Moreover, this approach holds promise for application to other energy systems. Given the growing importance of long-term energy flexibility, further exploration of the combination of offline SDDP with other optimization methods is highly interesting.

5.2 Limitations and future work

The research presented in this thesis has made significant contributions to the understanding and control of Power-to-Hydrogen(-to-Power) systems. However, there are certain limitations that need to be

addressed in future work.

While the application of Stochastic Dual Dynamic Programming (SDDP) has yielded promising results, there are some limitations that should be considered. The scenario tree was not validated against real-world data, so it might not accurately represent real scenarios. Furthermore, the use of more historical data is necessary to prevent overfitting. By incorporating a larger dataset, the accuracy and reliability of the terminal cost functions can be enhanced. At the same time, incorporating more historical data rows with the current method might be computationally intractable. Therefore, directly using statistical models electricity prices and solar irradiation might have higher potential. The creation of these models should be automatized since developing these models is very complex and time-intensive.

Additionally, evaluating the accuracy of the terminal cost function derived from SDDP is essential, especially considering the discrepancy that arises from the requirement of SDDP to be a LP while the Optimal Control Problem is a MILP. An inaccurate terminal cost function could lead to sub-optimal use of long-term flexibility.

Although the proposed MPC approach has demonstrated promising results, there are areas for improvement and future exploration. The first steps would be to apply stochastic MPC as was done in [23]. Additionally, it would be interesting to validate the control algorithm by running experiments on the real system. Lastly, it would be interesting to explore more nesting of optimization method, timestep sizes and model detail levels. This could improve solve time while allowing more accurate models where relevant.

Regarding the flexibility envelope, the worst case scenario for power minimization should be identified in a more sophisticated way, as it is currently heuristic. Furthermore, the reaction time of the electrolyser should be communicated with the system operator in addition to the flexibility envelope. Lastly, it would be interesting already include *Flexibility for Power* in the MPC algorithm, so that *Flexibility for Power* and *Flexibility for Energy* are optimized simultaneously. However, this would require a renumeration scheme for *Flexibility for Power* first.

Generally, it would be interesting to explore more systems, such as a Power-to-Hydrogen-to-Power system in a building. In this case, the hydrogen storage would be used on a more seasonal timescale. It would be interesting to explore different storage sizes and device capacities. Also, it would be very important to include the waste heat stream from the system in the model, as this can be a valuable energy source. Lastly, it would be interesting to not only use economic objective functions but to include CO2 emissions by using a CO2 price.

Bibliography

- [1] R. J. Aguiar, M. Collares-Pereira, and J. P. Conde. “Simple procedure for generating sequences of daily radiation values using a library of Markov transition matrices”. In: *Solar Energy* 40.3 (Jan. 1988), pp. 269–279. ISSN: 0038-092X. DOI: **10.1016/0038-092X(88)90049-7**.
- [2] Feras Alshehri et al. “Modelling and evaluation of PEM hydrogen technologies for frequency ancillary services in future multi-energy sustainable power systems”. In: *Heliyon* 5.4 (Apr. 2019). ISSN: 24058440. DOI: **10.1016/j.heliyon.2019.e01396**.
- [3] Richard E. Bellman. *Dynamic Programming*. 2003.
- [4] Darryl R Biggar and Mohammad Reza Hesamzadeh. *The Economics of Electricity Markets*. IEEE Press and John Wiley & Sons Ltd, 2014.
- [5] J. M. Bright et al. “Stochastic generation of synthetic minutely irradiance time series derived from mean hourly weather observation data”. In: *Solar Energy* 115 (May 2015), pp. 229–242. ISSN: 0038092X. DOI: **10.1016/J.SOLENER.2015.02.032**.
- [6] Alexander Buttler and Hartmut Spliethoff. *Current status of water electrolysis for energy storage, grid balancing and sector coupling via power-to-gas and power-to-liquids: A review*. Feb. 2018. DOI: **10.1016/j.rser.2017.09.003**.
- [7] Hanmin Cai and Philipp Heer. “Experimental implementation of an emission-aware prosumer with online flexibility quantification and provision”. In: (Oct. 2021). URL: **<http://arxiv.org/abs/2110.12831>**.
- [8] Conference of the Parties. “Adoption of the Paris Agreement”. In: *Report of the Conference of the Parties on its twenty-first session, held in Paris from 30 November to 13 December 2015*. Paris, Dec. 2016.
- [9] Georgios ; Darivianakis et al. “A Data-Driven Stochastic Optimization Approach to the Seasonal Storage Energy Management”. In: (2017). DOI: **10.3929/ethz-b-000231975**. URL: **<https://doi.org/10.3929/ethz-b-000231975>**.
- [10] Anthony Downward, Oscar Dowson, and Regan Baucke. “Stochastic dual dynamic programming with stagewise-dependent objective uncertainty”. In: *Operations Research Letters* 48.1 (Jan. 2020), pp. 33–39. ISSN: 0167-6377. DOI: **10.1016/J.ORL.2019.11.002**.
- [11] Oscar Dowson. *An introduction to SDDP.jl*. URL: **https://odow.github.io/SDDP.jl/stable/tutorial/first_steps/**.
- [12] Oscar Dowson and Lea Kapelevich. “SDDP.jl: A Julia Package for Stochastic Dual Dynamic Programming”. In: **<https://doi.org/10.1287/ijoc.2020.0987>** 33.1 (Aug. 2020), pp. 27–33. ISSN: 15265528. DOI: **10.1287/IJOC.2020.0987**. URL: **<https://pubsonline.informs.org/doi/abs/10.1287/ijoc.2020.0987>**.
- [13] Mehdi Ghazavi Dozein, Antonella Maria De Corato, and Pierluigi Mancarella. “Virtual Inertia Response and Frequency Control Ancillary Services From Hydrogen Electrolyzers”. In: *IEEE Transactions on Power Systems* (2022). ISSN: 15580679. DOI: **10.1109/TPWRS.2022.3181853**.
- [14] ENTSO-E. *ENTSO-E Transparency Platform*. URL: **<https://transparency.entsoe.eu/>**.
- [15] Benjamin Flamm et al. *Dual Dynamic Programming for Nonlinear Control Problems over Long Horizons; Dual Dynamic Programming for Nonlinear Control Problems over Long Horizons*. 2018. ISBN: 9783952426999. DOI: **10.0/Linux-x86{_}64**.
- [16] Jan Gasser et al. “Predictive energy management of residential buildings while self-reporting flexibility envelope”. In: *Applied Energy* 288 (Apr. 2021). ISSN: 03062619. DOI: **10.1016/j.apenergy.2021.116653**.
- [17] F. Grüger et al. “Optimized electrolyzer operation: Employing forecasts of wind energy availability, hydrogen demand, and electricity prices”. In: *International Journal of Hydrogen Energy* (Feb. 2019), pp. 4387–4397. ISSN: 03603199. DOI: **10.1016/j.ijhydene.2018.07.165**.

- [18] Emil Hillberg et al. *Power Transmission & Distribution Systems Flexibility needs in the future power system Discussion paper Disclaimer*. Tech. rep. International Smart Grid Action Network, Mar. 2019.
- [19] C Hodel. *Overview of Ancillary Services*. Tech. rep. Aarau: Swissgrid, Sept. 2019.
- [20] Matthieu Jonin et al. “Exergy-based model predictive control for design and control of a seasonal thermal energy storage system”. In: *Journal of Physics: Conference Series*. Vol. 1343. 1. Institute of Physics Publishing, Nov. 2019. DOI: [10.1088/1742-6596/1343/1/012066](https://doi.org/10.1088/1742-6596/1343/1/012066).
- [21] Binod Koirala et al. “Integrated electricity, hydrogen and methane system modelling framework: Application to the Dutch Infrastructure Outlook 2050”. In: *Applied Energy* 289 (May 2021). ISSN: 03062619. DOI: [10.1016/j.apenergy.2021.116713](https://doi.org/10.1016/j.apenergy.2021.116713).
- [22] Josien de Koning. “Flexibility Assessment of Residential Power-to-Hydrogen-to-Power System with Seasonal Storage”. PhD thesis. 2022.
- [23] Timo Laaksonlaita. “Modelling, Identification and Control of a Renewable Hydrogen Production System for Mobility Application”. PhD thesis. 2021.
- [24] Brahim Laoun et al. “Modeling of solar photovoltaic-polymer electrolyte membrane electrolyzer direct coupling for hydrogen generation”. In: *International Journal of Hydrogen Energy* 41.24 (June 2016), pp. 10120–10135. ISSN: 03603199. DOI: [10.1016/j.ijhydene.2016.05.041](https://doi.org/10.1016/j.ijhydene.2016.05.041).
- [25] Jose Daniel Lara et al. “A Multi-Stage Stochastic Risk Assessment with Markovian Representation of Renewable Power”. In: *IEEE Transactions on Sustainable Energy* 13.1 (Jan. 2022), pp. 414–426. ISSN: 19493037. DOI: [10.1109/TSTE.2021.3114615](https://doi.org/10.1109/TSTE.2021.3114615).
- [26] Eric W. Lemmon, Marcia L. Huber, and Jacob W. Leachman. “Revised Standardized Equation for Hydrogen Gas Densities for Fuel Consumption Applications”. In: *Journal of Research of the National Institute of Standards and Technology* 113.6 (2018), pp. 341–350. DOI: [10.6028/jres.113.028](https://doi.org/10.6028/jres.113.028).
- [27] Han Li et al. *Energy flexibility of residential buildings: A systematic review of characterization and quantification methods and applications*. Aug. 2021. DOI: [10.1016/j.adapen.2021.100054](https://doi.org/10.1016/j.adapen.2021.100054).
- [28] Benjamin Lux and Benjamin Pfluger. “A supply curve of electricity-based hydrogen in a decarbonized European energy system in 2050”. In: *Applied Energy* 269 (July 2020). ISSN: 03062619. DOI: [10.1016/j.apenergy.2020.115011](https://doi.org/10.1016/j.apenergy.2020.115011).
- [29] Portia Murray. “The Role of Power-to-X Technologies in Decentralised Multi-Energy Systems”. PhD thesis. ETH Zürich, 2020.
- [30] Nationaal Waterstof Programma. *Hydrogen Roadmap for the Netherlands*. Tech. rep. URL: www.nationaalwaterstofprogramma.nl.
- [31] Sayyad Nojavan, Kazem Zare, and Behnam Mohammadi-Ivatloo. “Application of fuel cell and electrolyzer as hydrogen energy storage system in energy management of electricity energy retailer in the presence of the renewable energy sources and plug-in electric vehicles”. In: *Energy Conversion and Management* 136 (2017), pp. 404–417. ISSN: 01968904. DOI: [10.1016/j.enconman.2017.01.017](https://doi.org/10.1016/j.enconman.2017.01.017).
- [32] M V F Pereira and L M V G Pinto. *Multi-stage stochastic optimization applied to energy planning*. Tech. rep. 1991, pp. 359–375.
- [33] Christian Peter, Evangelos Vrettos, and Felix N. Büchi. “Polymer electrolyte membrane electrolyzer and fuel cell system characterization for power system frequency control”. In: *International Journal of Electrical Power & Energy Systems* 141 (Oct. 2022), p. 108121. ISSN: 0142-0615. DOI: [10.1016/J.IJEPES.2022.108121](https://doi.org/10.1016/J.IJEPES.2022.108121).
- [34] Steffen Rebennack. “Combining sampling-based and scenario-based nested Benders decomposition methods: application to stochastic dual dynamic programming”. In: *Mathematical Programming* 156.1-2 (Mar. 2016), pp. 343–389. ISSN: 14364646. DOI: [10.1007/S10107-015-0884-3](https://doi.org/10.1007/S10107-015-0884-3). URL: <https://link.springer.com/article/10.1007/s10107-015-0884-3>.
- [35] Arash E. Samani et al. “Grid balancing with a large-scale electrolyser providing primary reserve”. In: *IET Renewable Power Generation* 14.16 (Dec. 2020), pp. 3070–3078. ISSN: 17521424. DOI: [10.1049/iet-rpg.2020.0453](https://doi.org/10.1049/iet-rpg.2020.0453).
- [36] Schweizerische Eidgenossenschaft. *Strompreise Schweiz*. URL: <https://www.strompreis.elcom.admin.ch/>.
- [37] Stiftung Umwelt Arena Schweiz. *Architektur und Bauprojekte*. URL: <https://www.umweltarena.ch/ueber-uns/architektur-und-bauprojekte/>.
- [38] Zheng Tian et al. *Review on equipment configuration and operation process optimization of hydrogen refueling station*. Jan. 2022. DOI: [10.1016/j.ijhydene.2021.10.238](https://doi.org/10.1016/j.ijhydene.2021.10.238).

- [39] Lukas Weimann et al. “Optimal hydrogen production in a wind-dominated zero-emission energy system”. In: *Advances in Applied Energy* 3 (Aug. 2021). ISSN: 26667924. DOI: **10.1016/j.adapen.2021.100032**.
- [40] Reihaneh Haji Mahdizadeh Zargar and Mohammad Hossein Yaghmaee Moghaddam. “Development of a markov-chain-based solar generation model for smart microgrid energy management system”. In: *IEEE Transactions on Sustainable Energy* 11.2 (Apr. 2020), pp. 736–745. ISSN: 19493037. DOI: **10.1109/TSTE.2019.2904436**.
- [41] Cong Zhang et al. “Flexible grid-based electrolysis hydrogen production for fuel cell vehicles reduces costs and greenhouse gas emissions”. In: *Applied Energy* 278 (Nov. 2020). ISSN: 03062619. DOI: **10.1016/j.apenergy.2020.115651**.
- [42] Pengfei Zhang et al. “Optimized Economic Dispatching Approach for PEM Electrolyzer Cell Combined with Coal-fired Power Units to Participate in Frequency Regulation Service”. In: *Proceedings - 2021 International Conference on Power System Technology: Carbon Neutrality and New Type of Power System, POWERCON 2021* (2021), pp. 395–400. DOI: **10.1109/POWERCON53785.2021.9697483**.